ENVIRONMENTAL FRIENDLY INHIBITORS FOR CO_2 CORROSION

BY

ABDULLAH AHMED ALAHMARY

A Thesis Presented to the

DEANSHIP OF GRADUATE STUDIES

KING FAHD UNIVERSITY OF PETROLEUM & MINERALS

DHAHRAN, SAUDI ARABIA

In Partial Fulfillment of the
Requirements for the Degree of

MASTER OF SCIENCE

In

MECHANICAL ENGINEERING

November 2015

KING FAHD UNIVERSITY OF PETROLEUM & MINERALS

DHAHRAN-31261, SAUDI ARABIA

DEANSHIP OF GRADUATE STUDIES

This thesis, written by **Abdullah Ahmed AlAhmary** under the direction his thesis advisor and approved by his thesis committee, has been presented and accepted by the Dean of Graduate Studies, in partial fulfillment of the requirements for the degree of **MASTER OF SCIENCE IN MECHANICAL ENGINEERING.**

Dr. Zuhair M. Gasem
(Advisor)

Dr. Zuhair M. Gasem
Department Chairman

Dr. Saviour Umoren
(Co-Advisor)

Dr. Salam A. Zummo
Dean of Graduate Studies

Dr. Ihsan ul Haq Toor
(Member)

4/1/16
Date

Dr. Syed Fida Hassan
(Member)

Dr. Yahya T. Al-Janabi
(Member)

© Abdullah Ahmed AlAhmary

2015

Dedication

This is dedicated to my brilliant and outrageously loving and supportive wife, Ashwaq Shafloot, our exuberant, sweet, and kind-hearted little girl, Lujain Alahmary, and to my always encouraging, ever faithful brother and sister, Abdumajeed and Ibtesam Alahmary.

ACKNOWLEDGMENTS

Acknowledgment is due to the King Fahd University of Petroleum & Minerals for supporting this research.

I wish to express my appreciation to Dr. Zuhair Gasem, who served as my major advisor, and Dr. Saviour Umoren, who served as my co-advisor. I also wish to thank the rest of my thesis committee, Dr. Ihsan ul Haq Toor, Dr. Syed Fida Hassan, and Dr. Yahya Janabi.

TABLE OF CONTENTS

LIST OF TABLES

LIST OF FIGURES

ABSTRACT

Full Name : [Abdullah Ahmed Awdhah Al Shafloot AlAhmary]

Thesis Title : [Environmental Friendly Inhibitors for CO2 Corrosion]

Major Field : [Master of Science in Mechanical Engineering]

Date of Degree : [November 2015]

The performances of two green inhibitors (chitosan and carboxymethyl cellulose (CMC)) and one commercial inhibitor on a typical X60 pipeline steel in CO_2-saturated saline solution were investigated in both static and dynamic conditions using electrochemical impedance spectroscopy (EIS) and potentiodynamic polarization (PDP) techniques. The results showed marked effects of inhibitor concertation, temperature, exposure time, and dynamic flow on the inhibition efficiency of each inhibitor. The inhibition efficiency increased with increases in chitosan and CMC concentrations. The inhibition efficiency degraded as the temperature increased from 25 to 40^{o}C and then improved as the temperature was raised to 60^{o}C for all inhibitors investigated with better performance of the commercial inhibitor compared to chitosan and CMC. The inhibition efficiency of chitosan and the commercial inhibitor improved with longer exposure time while that of CMC decreased. Potentiodynamic polarization measurements suggested that both inhibitors essentially acted as mixed-type inhibitors. A rotating cylinder electrode (RCE) was used to study the rate of corrosion under flow condition. The results revealed that the inhibition efficiency of chitosan decreased under flow condition while the same increased for CMC. The adsorption isotherm of both environment friendly inhibitors obeyed Langmuir's isotherm.

Keywords: Chitosan, Carboxymethyl Cellulose, X60 Steel, Rotating Cylinder Electrode

ملخص الرسالة

الاسم الكامل: عبدالله بن احمد بن عوضه ال شفلوت الاحمرى

عنوان الرسالة: مثبطات التآكل المصاحبة للبيئة لغاز ثاني أكسيد الكربون

التخصص: درجة الماجستير في العلوم في الهندسة الميكانيكية

تاريخ الدرجة العلمية: تشرين الثاني لعام 2015

تم دراسة اثنين من مثبطات التآكل المصاحبة للبيئة، الشيتوزان و السليلوز كربوكسي ميثيل، بالإضافة إلى مثبط آخر تجاري وكان ذلك على خط أنابيب مصنوع من الفولاذ في محلول ملحي مشبع بغاز ثاني أكسيد الكربون تحت كلا من الظروف الساكنة والديناميكية، وذلك باستخدام تقنية الكهروكيميائية مقاومة الطيفي (Electrochemical Impedance Spectroscopy) وتقنية الاستقطاب عند جهد ديناميكي (Potentiodynamic Polarization). ولقد أظهرت النتائج مدى تأثير كلا من تركيز المثبط و درجة الحرارة ووقت الغمر و التدفق الديناميكي على كفاءة التثبيط. لقد ارتفعت كفاءة التثبيط مع ارتفاع تركيز كلا من الشيتوزان والسليلوز كربوكسي ميثيل. كما أنها انخفضت مع ارتفاع درجة الحرارة من ٢٥ إلى ٤٠ درجة مئوية ومن ثم ارتفعت مع ارتفاع درجة الحرارة إلى ٦٠ درجة مئوية وكان أداء المثبط التجاري أفضل مقارنة بالشيتوزان والسليلوز كربوكسي ميثيل. كان هناك أيضا تحسن في كفاءة التثبيط لكلا من الشيتوزان والمثبط التجاري عند زيادة وقت الغمر في حين انخفض الأداء في وجود السليلوز كربوكسي ميثيل. وتشير قياسات الاستقطاب عند جهد ديناميكي أن كل المثبطات تعمل أساسا من نوع مثبطات مختلطة. وقد استخدم القطب الكهربائي للاسطوانة الدوارة (Rotating Cylinder Electrode) لدراسة معدل التآكل في ظل ظروف التدفق، وكشفت النتائج أن كفاءة تثبيط الشيتوزان انخفضت في ظل الظروف الديناميكية، في حين أن كفاءة تثبيط السليلوز كربوكسي ميثيل زادت تحت نفس الظروف، الادمصاص من كل مثبط على السطح يسير وفق الأيزوثيرم لانجمير للإدمصاص.

CHAPTER 1

INTRODUCTION

Carbon steels are widely used in the petroleum industry for different purposes. Even though these materials have limited corrosion resistance, due to economic reasons they are preferred over other materials [1]. Depending on their fabrication process and chemical composition, these steels may have different microstructures that could affect their mechanical properties and corrosion resistance [2].

Among the most frequent and aggressive environments found in the oil and gas industry are fluids with high concentrations of chlorides containing carbon dioxide [3]. Carbon dioxide corrosion, also referred to as "sweet corrosion," involves the interaction between steel, water, and CO_2 [4]. One of the most cost-effective methods for controlling carbon dioxide corrosion during oil and gas production is the use of chemical corrosion inhibitors. "Corrosion inhibitors" are basically chemical compounds that form a protective layer on a metal when added to a gas or liquid and that consequently result in reduced corrosion rate. There is an increasing need in the industry to limit the use of chemicals (mainly due to more severe environmental constraints) and to search for greener products [1]. In order to comply with environmental restrictions worldwide,

chemical suppliers have developed environmentally friendly production chemicals, either by reformulating existing products or by identifying new chemistries for developing new products.

Several green chemicals have been reported in the literature, including scale inhibitors, demulsifers, and corrosion inhibitors [5-7]. Our interest is in the environmentally friendly (green) corrosion inhibition for CO_2 corrosion. In this study, the performance of two green inhibitors—chitosan and carboxymethyl cellulose (CMC), as single-component inhibitors on a typical X60 pipeline steel in CO_2-saturated 3.5% NaCl solution—are investigated in both static and dynamic conditions; these green inhibitors are compared to a commercial inhibitor, using electrochemical impedance spectroscopy (EIS) and potentiodynamic polarization (PDP) techniques. In addition, metal surface characterization is performed using a scanning electron microscope (SEM).

CHAPTER 2

LITERATURE REVIEW

A literature review was conducted for this thesis with two main themes: carbon dioxide corrosion and corrosion inhibition. The literature review below reflects the current understanding of these two areas, and helps in identifying gaps in knowledge as they relate to this particular research topic.

2.1 Carbon Dioxide Corrosion

2.1.1 Carbon Dioxide Corrosion: Its Mechanisms

Carbon dioxide corrosion has emerged as a common and costly problem in the oil and gas industry, given that oil and gas from oil fields and gas wells generally contain some level of CO_2. This factor has attracted a great deal of research and scrutiny over the years. The primary concern about CO_2 corrosion in the oil and gas industry is that it can potentially result in failure of equipment and pipelines, which thus can disrupt oil/gas production and transportation [8]. Research on CO_2 over the course of several decades has provided insights into its reaction and properties. The chief chemical function that takes place is the dissolution and hydration of CO_2, which causes carbonic acid to form. Equations 2.1 and 2.2, below, illustrate this behavior:

$$CO_{2_{(g)}} \rightarrow CO_{2_{(aq)}} \quad (2.1)$$

$$CO_{2_{(aq)}} + H_2O \rightarrow H_2CO_{3_{(aq)}} \quad (2.2)$$

"Acid corrosion" is another term used for CO_2 corrosion due to the formation of weak carbonic acid which, when compared with strong acids such as sulfuric acid (H_2SO_4) or hydrochloric acid (HCl), dissociates partially in water [4].

The carbonic acid goes through two steps to dissociate into bicarbonate and carbonate. Equations 2.3 and 2.4 illustrate these steps:

$$H_2CO_{3_{(aq)}} \rightarrow H^+ + HCO_3^- \quad (2.3)$$

$$HCO_3^- \rightarrow H^+ + CO_3^{2-} \quad (2.4)$$

An electrochemical reaction—CO_2 corrosion—is illustrated in Equation 2.5 in its overall response:

$$Fe + CO_2 + H_2O \rightarrow FeCO_3 + H_2 \quad (2.5)$$

A corrosion product, iron carbonate ($FeCO_3$), develops while CO_2 corrosion takes place; it can precipitate on the steel surface, or it can remain dissolved [9]. On the steel surface, the electrochemical responses include the anodic dissolution of iron, as illustrated in Equation 2.6:

$$Fe \rightarrow Fe^{2+} + 2e^- \quad (2.6)$$

Although extensive research has been conducted over the past few years, which of the two cathodic reactions (Equations 2.7 or 2.8) actually take place on the metal surface

is not yet fully understood. Thus, it is presumed that the sum of the two cathodic reactions is the net cathodic current. Researchers have also postulated that the bicarbonate ions, upon direct reduction, become significant at greater pH levels [10].

$$2H^+ + 2e^- \rightarrow H_2 \quad (2.7)$$

$$2H_2CO_3 + 2e^- \rightarrow H_2 + 2HCO_3^- \quad (2.8)$$

2.1.2 Types of Carbon Dioxide Corrosion

The following four types of corrosion may be caused by CO_2:

- Pitting corrosion
- Mesa attack
- Flow-induced corrosion
- General uniform corrosion

Pitting, or localized corrosion, has been known since the early days of research on CO_2 corrosion, and researchers have continued to investigate this type of corrosion [11-14]. As illustrated in Figures 1 to 3, pitting is quite difficult to predict and is often found in small areas that are prone to heavy attack. Deep cavities are formed as a result, and at a considerably higher corrosion rate. One explanation for this process in the literature is that pitting might be triggered by a local electrochemical concentration cell between the pipe surface and the pit cavity [3]. The American Society of Mechanical Engineers' (ASME's) B31G method is often used in the oil and gas industry to assess the lifetime of pipelines that are attacked by pitting [15].

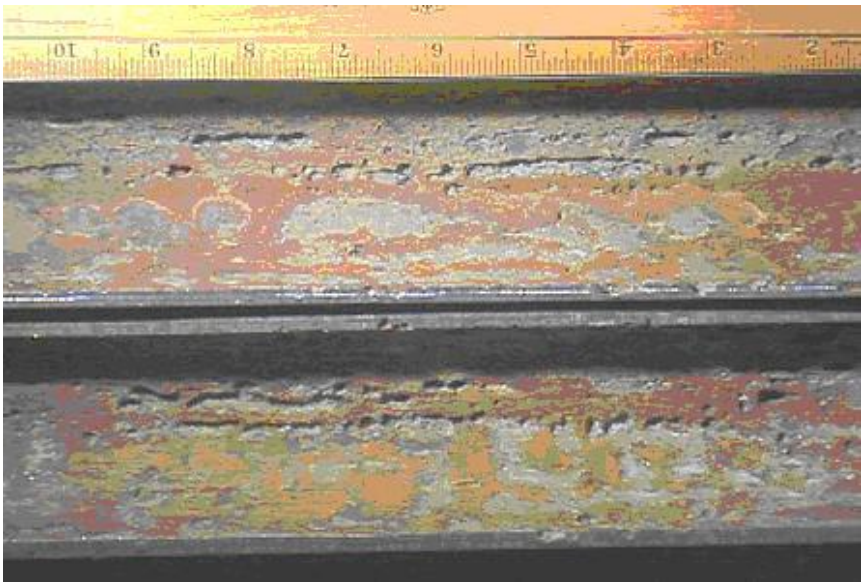

Figure 1: CO_2 corrosion of a carbon steel oil and gas production flow line [16].

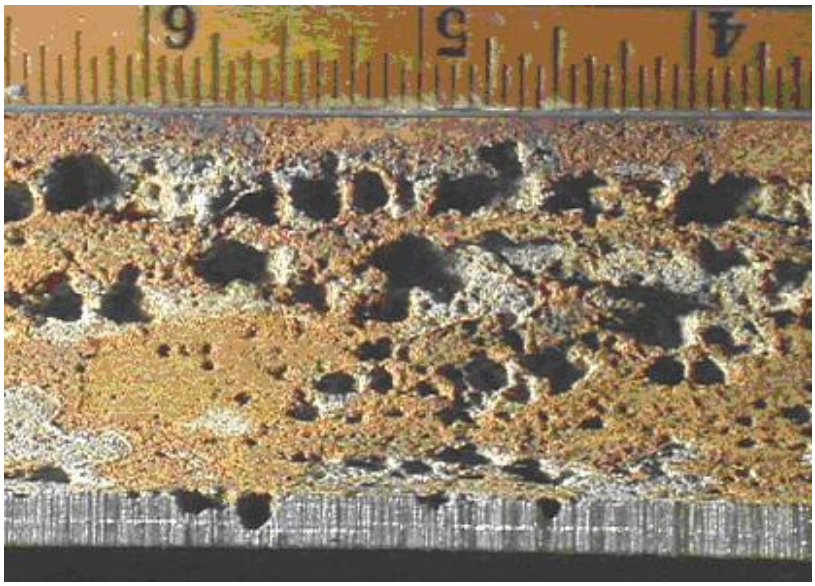

Figure 2: Higher magnification view of the corrosion pits shown in Figure 1 [16].

Figure 3: CO_2 corrosion of carbon steel pipe nipple in CO_2-contaminated water [16].

"Mesa attack" (Figure 4) is another type of CO_2 corrosion, which is similar in nature to pitting corrosion but that occurs at higher flow rates [17,18]. The process was not clear until the late 1990s, however, when Nyborg used a video camera to capture the process and proposed the mechanism illustrated in Figure 5 [19]. Mesa attack is initiated by the iron dissolution beneath the corrosion product, which the latter breaks at a certain point and is removed by the high flow rate. This process—the dissolution and removal of the corrosion film—is a continuous process that leads to high corrosion rates that are equivalent to normal pitting [3].

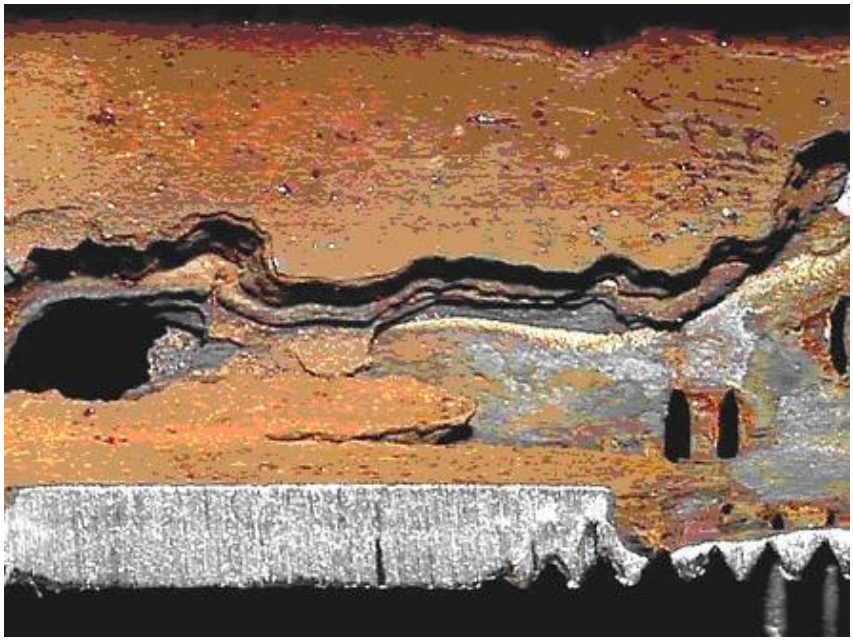

Figure 4: An inside view of the nipple in Figure 3, showing "mesa"-type corrosion typical of CO_2 corrosion [16].

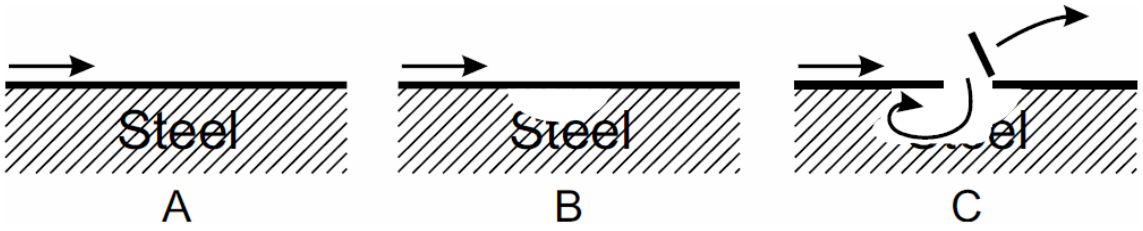

Figure 5: Mesa attack illustration: A: High flow rate. B: Iron dissolution under corrosion product. C: Breaking off of corrosion product, and more iron dissolution. This results in the continual breaking off of the corrosion product [3].

2.1.3 Factors Affecting Carbon Dioxide Corrosion

Quite a few important factors that control CO_2 corrosion have been identified, including, but not limited to, water chemistry, temperature, and fluid flow. Each of these three factors is discussed below.

2.1.3.1 The Effect of Water Chemistry

A primary component of CO_2 corrosion is water chemistry, which normally involves pH level, iron carbonate film formation, and other types of scale formation. CO_2 produces many species in water, such as carbonate ions, hydronium ions, carbonic acid, and bicarbonate ions. Their dissolution rate can be measured by solving the equilibria of the chemical reactions with an electroneutrality equation for open systems (constant CO_2 partial pressure), and/or a carbonic species conservation equation for closed systems (varied CO_2 partial pressure). Aqueous-solution pH can be calculated with a few available parameters such as temperature, partial pressure of CO_2, and total pressure [4]. Higher pH normally results in lower corrosion rates, by decreasing the solubility of iron carbonate; this leads to the faster formation of protective films [8].

2.1.3.2 The Effect of Temperature

In CO_2 corrosion, all of the involved processes, electrochemical reactions on the metal surface, the transport of species, and chemical reactions in the bulk of the solutions, can be accelerated by temperature. The development of an iron carbonate film is temperature-dependent. Depending on the pH level and the solubility of the protective film, the temperature may increase or decrease the corrosion rate significantly. At lower pH levels, the increase in temperature will lead to higher precipitation rates and faster film formation, and hence reduction in corrosion rates. On the other hand, corrosion rates will increase with increasing temperature if the protective films do not form (usually at high pH) [8].

2.1.3.3 The Effect of Flow

The cathodic reaction–limiting current involves two components: a flow-independent component (hydration of CO_2) and a flow-dependent component (diffusion of H^+ and H_2CO_3). The corrosion rate usually depends on the type of flow: whether it is a single- or multi-phase water flow. For the former, the corrosion rates increase with increased flow velocity due to the enhancement of the corrosive species' mass transfer rate from the bulk solution to the steel surface, and the corrosion product species away from the steel surface to the bulk solution. If either the corrosion inhibitor film or the protective scale ($FeCO_3$) forms on the steel surface, flow might not have a significant impact on the uniform corrosion rates. Turbulent flow may, however, mechanically remove the protective scale or film, such as in flanges, bends, valves, and weld beads [4].

When compared to single-phase flow, and due to the different flow patterns and phase-wetting regimes, the multi-phase flow makes both experimental and modeling work on CO_2 corrosion complicated. Because water wetting on the steel surface is one of the main reasons for internal pipeline corrosion, corrosion can be considerably lessened (or even avoided entirely) if water is entrained in the flowing oil phase [4].

2.2 CO_2 Corrosion Inhibition

Corrosion inhibition is a complicated subject in the oil and gas industry that demands significant reliance on inhibitors when considering applications like wells, refineries, pipelines, or recovery units. The issue of inhibition in wells is further complicated by aggressive gasses like H_2S, CO_2, and organic acids [20]. "Corrosion inhibitors" are basically chemical compounds that form a protective layer on a metal when added to a gas or liquid and that consequently result in reduced corrosion rate. These inhibitors,

given their properties of absorption, are also referred to as “adsorption site blockers,” “site-blocking elements,” or “blocking species.” Inhibitors that are biocompatible in nature are referred to as “eco-friendly” or “green inhibitors,” and can be grouped into two main categories: inorganic green inhibitors and organic green inhibitors [21,22].

A wide range of polymers have been studied because of their excellent adsorption properties on metal surfaces; they have been found to have good anti-corrosive properties in the form of both inhibitors in corrosive fluids and/or the pre-coating on the metal surface (Table 1) [22]. In order to compare the inhibition efficiencies of synthetic and natural polymers, Umoren et al. (2008) studied polyethylene glycol and gum arabic for the corrosion inhibition of mild steel in sulfuric acid solutions; they also studied the synergistic effects of halide derivatives [23]. In addition, the authors have investigated the inhibitive properties of exudate gum for aluminum corrosion inhibition in acidic medium [24]. Although the time dependence of the inhibition efficiencies of the gum exudates followed a similar trend to gum arabic in their study, the effect of temperature was not the same. The inhibition efficiency increased on the temperature scale for the former, whereas it decreased for the latter. The authors therefore proposed that the gum exudates had physically adsorbed onto the surface of the aluminum.

Cellulose is the most abundant water-insoluble natural polysaccharide. Carboxymethyl cellulose (Figure 6) is a water-soluble synthetic analog of cellulose. Several studies have investigated the anti-corrosive properties of carboxymethyl cellulose (CMC) for mild steel in different acid solutions [25-27]. Chitosan (Figure 6) is a linear polysaccharide that is produced by the deacetylation of chitin, a naturally occurring polymer. Several articles have studied the effect of the degree of deacetylation on

properties such as solubility and antimicrobial activity [34,35]. Chitosan is widely used in a range of diverse fields, including medicine, textiles, paper, and food. While chitosan is rich in hydroxyl and amino groups, and thus is a good potential inhibitor, little has been reported about its inhibition behavior. Mahmoud et al. (2013) studied the behavior of copper in 0.5 M HCl acid containing different concentrations of chitosan; the investigated inhibitor showed good inhibition efficiency [36].

Table 1: List of natural polymers and derivatives studied as corrosion inhibitors [23,33].

Inhibitor	**Protected Metal**	**Medium**
Mimosa tannin	Low carbon steel	H_2SO_4
Guar gum	Carbon steel	H_2SO_4
Gum arabic	Mild steel	H_2SO_4
Exudate gums	Aluminum	HCl
Carboxymethyl cellulose	Mild steel	HCl
Hydroxyethylcellulose	Mild steel	HCl
Carboxymethyl cellulose	Mild steel	H_2SO_4
Starch	Mild steel	H_2SO_4
Chitosan	Copper	HCl

In general, eco-friendly inhibitors are excellent inhibitors for most metals under a wide range of corrosive environments. The major advantages of these inhibitors are their non-toxicity and biodegradability; they do have performance limitations, however, and further research efforts are needed before these inhibitors can be widely employed at the industrial level [36].

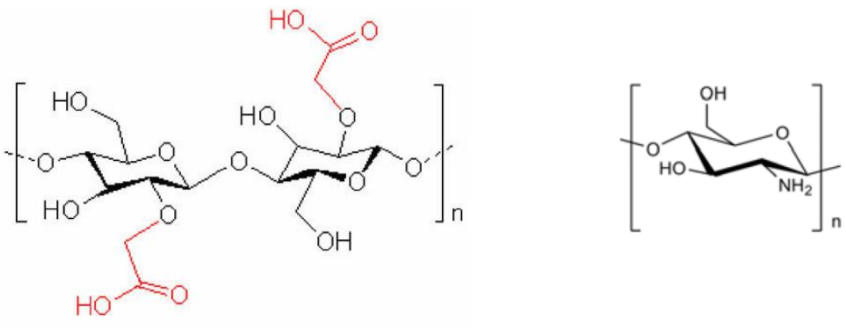

Carboxymethyl cellulose **Chitosan**

Figure 6: Chemical structure of CMC and Chitosan repeat units.

2.3 Review of Related Literature

Steel Structures used for oil and gas production and transportation facility fabrications have been heavily plagued by CO_2 corrosion; researchers worldwide have developed various corrosion control techniques to mitigate the problem. Wang et al. (2011) reported an EIS-based evaluation of the corrosion control performance of a new thioureidoimidazoline-type inhibitor for mild steel in CO_2-saturated saline solution [37]. The results revealed 0.15 mmol/dm^3 as the peak-value concentration for this compound on steel. Protonated thioureidoimidazoline species were reported to instill the needed attraction at the negatively charged substrate. The electrostatic forces between the atomic force microscopy (AFM) tip and the charged steel surface were studied for the potential of zero charge at the surface, as well as the reduction of the effect of surface charges. The authors also employed x-ray photoelectron spectroscopy (XPS) to show the different states of the adsorbed species on steel.

The effect of iodide addition on the corrosion inhibition performance of another imidazoline substituted derivative, amido-imidazoline (AIM), has been investigated in CO_2-saturated NaCl (3.0%) solution for American Petroleum Institute (API) 5L X52-

grade steel using electrochemical techniques [38]. The corrosion inhibition of this steel grade was found to synergistically increase with the amount of iodide ions in combination with amido-imidazoline compound; increased corrosion performance of this compound was found at higher concentrations. Its Tafel behavior proposed a mixed-type system, and its AIM adsorption was approximated with a Langmuir adsorption isotherm, with a chemical adsorption mechanism proposed at the range of the temperature under study.

Okafor et al. (2009) have also investigated the effect of iodide addition on the anticorrosive behavior of 2-undecyl-1-ethylamino imidazoline in CO_2-saturated NaCl (3.0%) solutions for mild steel (N80 grade) with electrochemical and surface analytical evaluation [39]. The imidazoline-derivative responded as a mixed-type inhibitor system for potentiodynamic polarization results, while improved corrosion performance was realized at higher concentrations of iodide ions and at increased temperatures. A Temkin isotherm was employed to approximate the compound's adsorption behavior in the presence of iodide ions. The activation energies in the presence and absence of the molecules of this inhibitor (as well as the iodide additive) were calculated to confirm the proposed chemisorption mechanism. The surface morphology of the substrate was studied using SEM, and the results were correlated with the EIS and Tafel experiments.

The mild steel corrosion inhibition ability of N-[2-[(2-aminoethyl)amino]ethyl]-9-octadecenamide in CO_2-saturated NaCl (5.0%) solution has been reported using chemical and electrochemical techniques [40]. The inhibitor's corrosion retardation strength was found to decrease with temperature, and not with its concentration relative to the critical micelle concentration. The inhibitor's adsorption on the steel surface was approximated

with a Frumkin adsorption isotherm. The physisorption adsorption mechanism stemmed from the activation energy and the thermodynamic parameters at reduced concentrations of the inhibitor, but reversed when the concentration increased.

Using rotating disk electrode (RDE) and square duct techniques, Ghareba and Omanovic (2011) have studied the effect of flow on carbon steel corrosion immersed in CO_2-saturated acidic solution containing 12-aminododecanoic acid [41]. Higher inhibition performances were realized at 3 mM, but lesser performances were realized at lower flow speeds and at lower concentrations of the inhibitor due to molecular desorption. The authors employed the impingement-jet configuration technique to complement the RDE and square duct methods.

Using electrochemical and surface analytical techniques, Nam et al. have reported on the anticorrosive performance of praseodymium 4-hydroxycinnamate in CO_2-saturated NaCl and naturally aerated solution for mild steel [42]. Using SEM, they revealed continuous growth of protective inhibitor film on the surface of the substrate. As revealed by the electrochemical results, the growth of the film increased with increased concentrations of the inhibitor at active electrochemical corrosion sites in the saline solution.

Jiang et al. (2005) have reported on quaternary alkynoxymethyl amine imidazolines as a corrosion inhibitor in CO_2-saturated saline solution for steel (N80 grade) in static and flowing conditions, using RDE for the latter [43]. They studied the effects of rotational speed and concentration of the inhibitors as they related to the inhibitors' performance using SEM, EIS, linear polarization resistance, and weight loss

techniques. The values of R_t and C_{dl} derived from EIS revealed 150 and 100 mg/L (for static and flow conditions) as the peak-value concentrations for these compounds below a 5 m/s flow rate. The adsorption of the inhibitor was approximated with Langmuir and Freundlich adsorption isotherms with a series of concentrations below and beyond 150 mg/L, respectively. The quaternary alkynoxymethyl amine imidazolines were better corrosion inhibitors at a 5 m/s flow speed.

Jevremovic et al. have reported on the corrosion inhibition performance of diethylenetriamine imidazoline in CO_2-saturated NaCl solutions for mild steel by using AFM and weight loss techniques [44]. They employed quartz crystal microbalance in studying the adsorption kinetics and the mechanism of the inhibitor (self-assembled monolayers) on Au electrodes, which were approximated with a Langmuir adsorption isotherm. The results from the chemical and surface topology revealed that the inhibitor reduced mild steel corrosion to a great extent by the formation of surface film.

Nam et al. (2013) have reported 4-carboxyphenylboronic acid's anticorrosive ability against steel in saline aqueous solution saturated with CO_2 using electrochemical techniques [45]. Low concentrations of compound reduced corrosion redox reactions and corrosion current densities, but they enhanced impedance and total (R_f and R_{ct}) resistances. SEM revealed uniform and smoother steel surfaces, which is indicative of protective film formation, and hence metal protection.

Jawich et al. (2012) have reported the corrosion inhibitive abilities of three new heptadecyl pendant-bearing imidazoline-substituted organic compounds against steel in saline (0.5 M NaCl) aqueous solution saturated with CO_2 using electrochemical

techniques [46]. The anticorrosive performance of these compounds was reported to be dependent on reaction temperature and the inhibitors' concentration. The experimental results revealed that 100 ppm was the peak-value concentration at 40°C for compounds I (diethylenetetramine-derived imidazoline), II (tetraethylenepentamine-derived imidazoline), and III (bis-imidazoline), with inhibition efficiency (IE%) of 84, 95, and 96 percent, respectively. The authors reported an optimum surface coverage on the steel substrate before attaining the peak-value concentration for the three inhibitors using SEM.

Three other imidazoline-type corrosion inhibitors (aminopropylimidazol and two commercial imidazoline-based products) have been reported for two carbon steel types (with annealed and tempered microstructures) in CO_2-saturated saline (5.0% NaCl) solution at pH of 6 and 40°C solution temperature using EIS and linear polarization resistance (LRP) [47]. The electrochemical results revealed that the annealed steel samples showed better resistance than the tempered steel in the solution of the electrolyte containing the commercially available products. The aminopropylimidazol formed a protective film on the surface of the steel, which was not observed for the other two products; this assertion was supported with the appearance of capacitive loops of the Nyquist curves from EIS as well as in the variation in phase angle shifts in the presence and absence of the corrosion inhibitors. The authors also proposed a mechanism of adsorption for three imidazoline-type corrosion inhibitors.

Khodyrev et al. (2011) have also investigated the anticorrosive behavior of dialkyldithiophosphoric acids in CO_2-saturated NaCl solutions for mild steel (N80 grade) with chemical, electrochemical, and surface analytical evaluation [48]. The corrosion

inhibitive performance (70–99 percent inhibition efficiency) was best at concentration ranges of 0.25–5 mg/l. The Tafel curves revealed that the inhibitors were mixed-type, with the absorption of the inhibitor molecules approximated with the Langmuir isotherm. The steel corrosion inhibition was found to be temperature- and concentration-dependent.

Using chemical and direct current (DC)–based electrochemical techniques, Zhao and Chen (2012) have reported the inhibition performance of sodium benzoate and oleic-based imidazoline in CO_2-saturated solution for mild steel [50]. From the EIS results, the inhibition of steel corrosion was found to be dependent on the immersion period, and greatly increased synergistically when two compounds were combined. EIS was also used in measuring the zero charge potentials of the substrate in the solution of the electrolyte in the presence and absence of the corrosion inhibitors. The authors also employed XPS in studying the elemental states of the adsorbed film.

Mazumder et al. conducted a study in which mild steel was further protected by p-(9-(2-methylisoxazolidin-5-yl)nonyloxy)benzaldehyde in CO_2-saturated (0.5 M NaCl) saline solution, studied at 40°C and 1 atm using chemical and electrochemical methods [51]. The anticorrosive performance of this compound was reported to be dependent on reaction temperature and inhibitor concentration. XPS results revealed that the inhibitor molecules adsorbed on the metal surface forming a thin film resulting in corrosion inhibition.

Mild steel has also been studied for its corrosion reduction properties using di- and tetraethylenetetramine-derived imidazoline-substituted (pendants) organic compounds in CO_2-saturated saline (0.5 M NaCl) solution at 40°C and 1 atm, using

weight loss and electrochemical analysis [52]. The corrosion inhibition of these pendants was linked with their unique electronic and molecular structures; the ring-nitrogen compounds revealed no protection to steel under the experimental conditions, while those compounds with an electron-rich aromatic ring coupled to amidine motifs showed remarkable corrosion inhibition. The authors also described an optimum surface coverage on the steel substrate before attaining the peak-value concentration for the three inhibitors using SEM, and XPS for the elemental state analysis.

Farelas and Ramirez have reported on (1-(2-hidroxyethyl)-2(heptadec-8-enyl)-imidazoline and 1-(2-aminoethyl)-2(heptadec-8-enyl)-bis-imidazoline for mild steel protection in CO_2-saturated saline (3% NaCl) solution at pH of 4 and 80°C solution temperature, using EIS and LRP under flowing conditions [53]. 1-(2-aminoethyl)-2(heptadec-8-enyl)-bis-imidazoline was found to be a better corrosion inhibitor (unaltered maximum IE% at 10 ppm) due to the compacted films it forms on the surface of the substrate at higher rotational speeds; this was characterized with EIS with the aid of RCE. The corrosion inhibition of steel was also enhanced at higher inhibitors' concentration and immersion time of the substrate in the solution of the electrolyte.

Sahin and Bilgic have investigated the anticorrosive behavior of 4-substituted triazole and amino-substituted diazole in CO_2-saturated NaCl (3.0%) solutions for carbon steel with a potentiodynamic polarization experiment [54]. The values of the corrosion current densities were found to decrease with the concentration of compounds. The corrosion inhibition of these pendants was linked with their unique electronic and molecular structures, planarity, aromaticity, and the presence of lone-pairs of electrons.

Using electrochemical methods, Okafor et al. (2010) have reported on the inhibition performance of 2-undecyl-1-sodium ethanoate-imidazoline salt and thiourea in CO_2-saturated (3.0% NaCl) solution for mild steel (N80 grade) in CO_2-saturated NaCl (3.0% NaCl) solutions at 25°C and pH of 4 [55]. The corrosion inhibition efficiency of mild steel was found to be concentration- and temperature-dependent. A mixed-type corrosion inhibitor system was proposed for both systems, while the steel protection mechanism in the presence of these compounds was ascribed to the formation of an adsorbed film on the surface of the steel substrate. 2-undecyl-1-sodium ethanoate-imidazoline salt and thiourea demonstrated a synergistic inhibiting action on steel protection, with their individual adsorption approximated with the Langmuir isotherm. Recent studies have reported on the application of sodium CMC and CMC, and the effect of halide ions in the presence of CMC, for steel corrosion inhibition [25-27]. Pure chitosan has been reported to inhibit acid-induced mild steel and copper corrosion [23,36]. Electrodeposition of chitosan and structurally modified chitosans have also been reported for the same application; acetyl thiourea chitosan and aminothiourea chitosans performed optimally in sulfuric acid medium [56-58].

CHAPTER 3

EXPERIMENTAL PROCEDURE

3.1 Materials

Inhibitors — Two green inhibitors (Chitosan and carboxymethyl-cellulose [CMC]) were compared to a commercial inhibitor.

Test fluids — Deoxygenated water that contained 3.5% NaCl and was CO_2-saturated.

Test coupon — A low carbon X60 steel, which is a typical pipeline steel, was tested (refer to Table 1 for coupon chemical composition). The tested coupon was in conformance with API X60 material specifications. The exposed area of the coupon was 1.323 cm^2 in static condition and 3.14 cm^2 in dynamic condition.

Table 2: Chemical composition of the tested coupon and its magnitude (%)

C 0.125	Si 0.52	Mn 1.83	P 0.0028	S 0.0044	Cr 0.121	Ni 0.091	Mo 0.079	Al 0.043	Cu 0.296
Co 0.0023	Ti 0.0058	Nb 0.053	V 0.078	W 0.134	Pb >0.030	B 0.0012	Sb <0.0010	Sn 0.081	Zn >0.032
As 0.0045	Bi <0.0015	Ta 0.0100	Ca 0.0059	Ce 0.0021	Zr <0.0015	La 0.029	Se <0.0020	N >0.019	Fe <96.2

3.2 Equipment

CO_2 corrosion inhibition experiments were conducted in a glass cell with a three-electrode setup (working, reference, and counter electrodes). Figure 7 shows a schematic of the glass cell test system set up in both dynamic and static conditions, with key

components marked and named. The fluid temperature was controlled by a Benchtop Temperature Controller. CO_2 gas was continuously bubbled through a gas dispersion tube into the cell to keep the water phase saturated with CO_2. An electrochemical technique was used to measure CO_2 corrosion rates with and without inhibition. A pH meter manufactured by Thermo-Scientific was used to monitor both the pH and the temperature.

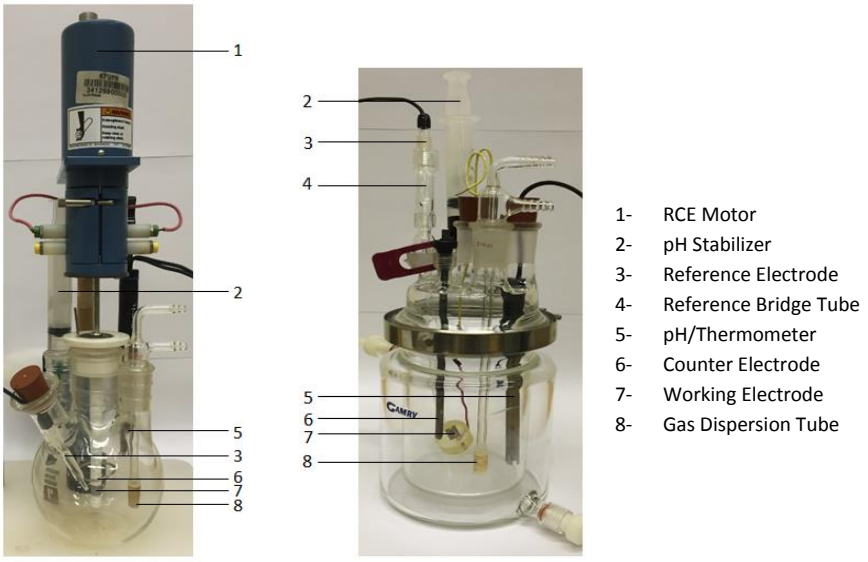

Figure 7: Schematic of glass cell setup used in dynamic and static conditions.

3.3 Sample Preparation

A low carbon X60 steel was tested; this is a typical steel used in pipelines. For the static condition, the test samples were cut in the form of disks with an area of 1.323 cm^2 and a thickness of about 1 mm, and then mounted with epoxy resin in a disk electrode holder. Surfaces were abraded initially with 120-, 240-, 320-, 400-, and 600-grit SiC paper, washed thoroughly with distilled water, degreased with ethanol, and air-dried. For the

dynamic condition, the test samples were cut in the form of cylinders with surface area of 3.14 cm^2 and wall thickness of 1 mm. The surfaces were polished with 400- and 600-grit SiC paper.

3.4 Inhibitor Evaluation

The objective of this study was to measure the inhibition efficiency of two green inhibitors (chitosan and carboxymethyl cellulose) as single-component inhibitors, and to compare them to a commercial inhibitor. This was accomplished by developing an understanding of the effects of several parameters: inhibitor concentration, solution temperature, turbulent flow conditions, and time of exposure on the corrosion rate of the tested material in both static and dynamic conditions. Tables 3 and 4 give the test parameters of the corrosion inhibition tests and the type of experiments conducted in the glass cell, respectively.

3.4.1 Inhibitor Evaluation under Static Conditions

The tested inhibitor was mixed with one liter of deionized water with 3.5% NaCl inside the glass cell. The solution was then purged with nitrogen (N_2) for thirty minutes to remove oxygen. After that, the solution was saturated with CO_2 for about ninety minutes. When the solution was saturated with CO_2, the pH was between 3.8 and 3.9. Since a pH of 5 is typical of the pH found in oilfields, this pH was selected in this work; this was achieved by the addition of a few drops of sodium bicarbonate ($NaHCO_3$). The working electrode was abraded with 400- and 600-grit SiC paper, washed thoroughly with distilled water, degreased with ethanol, and air-dried. After optimizing the test conditions, the working electrode was then immersed into the solution, and the tests were started.

Table 3: Test parameters of corrosion inhibition tests in the glass cell.

Working Electrode	Low carbon X60 steel
Counter Electrode	Graphite for static experiments and platinum for dynamic experiments
Reference Electrode	Saturated calomel electrode (SCE)
Partial Pressure of CO_2	≈13.0 psi
Solution	Deionized water with 3.5% NaCl
pH of Solution	5.0 (adjusted using sodium bicarbonate)

Table 4: List of experiments conducted.

	Specimen	Inhibitor Concentration (ppm)
Thirteen (13) experiments to study the effect of inhibitor concentration (T = 25°C, time of exposure = 1hr, static condition)	Blank	0
	Chitosan	25, 50, 75, 100
	CMC	25, 50, 75, 100
	Commercial	25, 50, 75, 100

	Specimen	Temperature (°C)
Twelve (12) experiments to study the effect of temperature (IC = 100ppm, time of exposure = 1hr, static condition)	Blank	25, 40, 60
	Chitosan	25, 40, 60
	CMC	25, 40, 60
	Commercial	25, 40, 60

	Specimen	Time of Exposure (hours)
Twelve (12) experiments to study the effect of time exposure (IC = 100ppm, T = 25°C, static condition)	Blank	1, 12, 24
	Chitosan	1, 12, 24
	CMC	1, 12, 24
	Commercial	1, 12, 24

	Specimen	Rotational Speed (rpm)
Eight (8) experiments to study the effect of rotational speed (IC = 100ppm, T = 25°C, time of exposure = 1hr, dynamic condition)	Blank	1,000; 1,500
	Chitosan	1,000; 1,500
	CMC	1,000;1,500
	Commercial	1,000; 1,500

3.4.2 Inhibitor Evaluation under Dynamic Conditions

The effectiveness of inhibitors for use under normally occurring flowing conditions is highly dependent upon the fluid velocity and the wall shear stresses. In order to characterize inhibitor performance under the flow conditions of pipelines, industry has adapted an RCE system for use in evaluating inhibitor performance. The performance of each inhibitor was evaluated at two rotating speeds (1,000 rpm and 1,500 rpm) under the same conditions for static testing.

3.4.3 Electrochemical Corrosion Rate Measurements

Two electrochemical techniques were used to measure the corrosion rates: electrochemical impedance spectroscopy (EIS) and potentiodynamic polarization (PDP). The techniques are briefly described here.

3.4.3.1 Electrochemical Impedance Spectroscopy (EIS)

Electrochemical Impedance Spectroscopy (EIS) experiments were performed under potentiostat condition between 100 kHz to 100mHz with a small amplitude perturbation (10 mV peak-to-peak) for an AC signal at E_{corr} using a Gamry Instrument potentiostat/galvanostat/ZRA (Reference 600/3000). The open circuit potential (also called “free corrosion potential”) was monitored to allow stable conditions to be reached (usually in 60 minutes). EIS measurements involve applying a small alternative potential to the electrode surface. The current response to the applied potential can differ in both phase and magnitude. Measuring the difference in phase and amplitude permits analysis of the electrode process in relation to contributions from diffusion, charge transfer, double layers, and inhibitor films. EIS offers several distinct advantages over conventional measurement methods such as linear polarization resistance (LPR). EIS is a

very useful tool for providing information on inhibitor film growth, and for generating parameters that are specific to a particular corrosion inhibitor system [30]. An equivalent electrical circuit model can provide a helpful way to interpret and qualify the EIS spectra if the physical models are understood.

3.4.3.2 Theoretical Background of EIS

Normally used in AC circuitries, impedance is the resistance to the flow of current when a minute amplitude sinusoidal excitation signal is applied across the system. The applied potential (E) is directly related to the values of the measured current (I) (via Equation 3.1 for simple circuits) but deviates slightly and becomes non-linear in complex AC circuits; impedance thus becomes the only quantity that defines the resistance of current flow in this system.

$$R = E/I \tag{3.1}$$

Across an electrochemical cell, the pseudo-linear current response (as expressed in Figure 3.1) is gradually measured across a defined range of frequencies, since it shifts in phase (∅) once a small amplitude perturbation has been applied. The potential (E) and current response (I) are now expressed in Equations 3.2 and 3.3, derived from Figure 8:

$$E_t = E_o \sin(\omega t) \tag{3.2}$$

$$I_t = I_o \, sin \, (\omega t + \emptyset) \tag{3.3}$$

Where E_o and I_o are the amplitudes of applied potential and current response, respectively, while ω is the angular frequency measured in radians per second (defined as $2\pi f$); ∅ and f are the phase separation/shift and the frequency of phase, respectively.

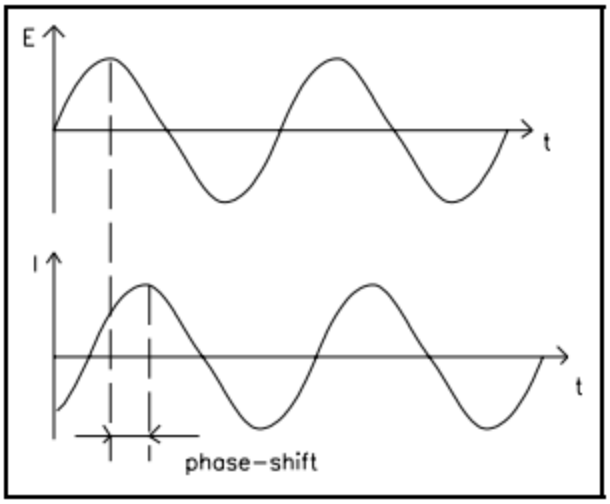

Figure 8: Sinusoidal I response typical in a linear system.

In complex non-linear circuits, by Ohm's Law, impedance (Z) can be redefined as ratios of applied potential and current response in terms of Z_o (Equation 3.4):

$$Z = \frac{E_t}{I_t} = \frac{E_o sin(\omega t)}{I_o \sin(\omega t + \emptyset)} = z_o \frac{\sin(\omega t)}{\sin(\omega t + \emptyset)} \tag{3.4}$$

The EIS technique relies on the fitting of experimental data-equivalent circuit models in electrochemical systems in order to define the Z value; depending on the circuit components, Z values are defined in different ways. For a resistor, for instance, Z is simply expressed as R, and is equivalent to $J\omega L$ and $1/J\omega C$ for inductor and capacitor, respectively. For circuits with electrical components in series, the equivalent impedance (Z_{eq}) is computed as expressed in Equation 3.5, and as expressed in Equation 3.6 for those with parallel circuit components:

$$Z_{eq} = Z_1 + Z_2 + Z_3 + \cdots + Z_n \tag{3.5}$$

$$Z_{eq} = \frac{1}{Z_1} + \frac{1}{Z_2} + \frac{1}{Z_3} + \cdots + \frac{1}{Z_n} \tag{3.6}$$

By using a potentiostat, the adequate voltage sweep within a defined frequency range is scanned across the electrochemical cell connected to it while the current response is

measured. A large range of data is normally collected, and several curves are plotted to compute for the resultant Z value. Experimental data can usually be represented in plots, that are not limited to Bode modulus and phase angle curves, showing a variation of impedance (Z_{mod} and Z_{phz}) with frequency; with the fitting of these data to equivalent circuit models, the corresponding values of each circuit component can be collected (resistance, capacitance, etc.).

3.4.3.3 Potentiodynamic Polarization

This technique is based on data obtained from cathodic and anodic polarization measurements. Cathodic data are preferred, since these are easier to measure experimentally. Potentiodynamic polarization studies were performed in this study in the potential range ±250 mV versus open circuit potential (E_{corr}) at a scan rate of 1 mVs^{-1}. To determine the corrosion rate (from the corrosion current density, i_{corr}) from such polarization measurements, the linear Tafel region of the polarization curve was extrapolated to the corrosion potential (Tafel's Assumption).

3.4.4 Metal Surface Characterization

The surface morphologies of four test specimens were also investigated, after twenty-four hours of exposure time with and without inhibitor, by using a scanning electron microscope (SEM).

3.4.5 Inhibition Efficiency

The corrosion inhibitor efficiency can be calculated using Equation 3.7, assuming that the K value of the system is the same constant with or without the presence of the inhibitor:

$$\%\ Inhibition = \frac{R_{p(CI)} - R_{p(B)}}{R_{p(CI)}} * 100\% \qquad (3.7)$$

where $R_{P(CI)}$ is the polarization resistance in the presence of the corrosion inhibitor; $R_{P(B)}$ is the polarization resistance of the blank. Besides the corrosion inhibitor efficiency, the inhibited corrosion rates are also considered in the evaluation of the inhibitor performance, as shown in Equation 3.8:

$$\%\ Inhibition = \frac{i_{corr_{(B)}} - i_{corr_{(CI)}}}{i_{corr_{(B)}}} * 100\% \quad (3.8)$$

where $i_{corr_{(CI)}}$ is the corrosion rate in the presence of the corrosion inhibitor, and $i_{corr_{(B)}}$ is the corrosion rate of the blank.

CHAPTER 4

RESULTS AND DISCUSSION

In this study, the performance of two green inhibitors—chitosan and carboxymethyl cellulose (CMC)— and one commercial inhibitor, on a typical X60 pipeline steel in CO_2-saturated 3.5% NaCl solution were investigated under both static and dynamic conditions, using electrochemical impedance spectroscopy (EIS) and potentiodynamic polarization (PDP) techniques. In addition, metal surface characterization was performed using a scanning electron microscope (SEM). The results and discussion will be provided in this chapter.

4.1 Effect of Inhibitor Concentrations

4.1.1 EIS Results

The effect of the amount of each inhibitor on the corrosion of X60 pipeline steel in 3.5% NaCl solution saturated with CO_2 was investigated using the EIS method at 25°C in order to examine the electrochemical process kinetics. The selected test frequency range for EIS was from 100 kHz to 100 MHz, with a 10 mV excitation amplitude at potentiostatic condition. Figures 9 and 10 present the one time-constant impedance spectra in the (a) Nyquist, (b) Bode, and (c) phase angle vs. frequency representations, respectively, in the presence and absence of varying concentrations of chitosan and CMC. Similar plots for the commercial inhibitor are presented in Figure 11. The Nyquist plots for the three

corrosion inhibitors show a similar curve shape, indicative of a similar mechanism of protection. These plots also reveal depressed full capacitive loops for all concentrations of chitosan and CMC over the range of frequency studied. Normally, larger diameters of Nyquist semi-circles are attributes of higher corrosion resistance systems of inhibitors compared to the blank solution. Higher concentrations of these inhibitors possess wider Nyquist curve widths. This electrochemical change is indicative of the corrosion inhibition process at increased concentrations of the inhibitors by adsorbing on the surface of the metal, thereby reducing the active surface area exposed to the aggressive corrosive electrolyte medium [59]. At lower frequencies for the blank solution alone, however, pseudo-inductive loops were observed, indicative of a possible negative change in the surface coverage due to relaxation of adsorption species typical of ions of the electrolyte (Cl^-) at the electrode surface [59, 60]. For the three inhibiting systems, the presence of the capacitive loop at medium and high frequencies suggests to the formation of a double electric layer due to corrosion inhibition [59]. Abd El Rehim has attributed this factor to a possible resistive nature of the interface caused by charge transfer resistance as a part of faradaic impedance [61]. The reason for the relative distortions of the semi-circles could be attributed to the unevenness of the metal surface; this phenomenon has been explained in details elsewhere [62].

In addition, higher impedance values for the Nyquist curves obtained were recorded for the commercial corrosion inhibitor to two folds of a thousand compared to chitosan and CMC. The reason for this varying superior resistance and protective performance in the presence of corrosive chloride ions and CO_2 could be due to the fact that chitosan and CMC are single-component substances, which are relatively small,

water-soluble, and linear polysaccharide compounds bearing simple amino and carboxymethyl groups, respectively, while the commercial inhibitor is an oil-based hybrid composite formulation consisting of active inhibitors, surfactant, enhancers, wetting agents, and modifiers in methanol. In our laboratory, we aim to develop a corrosion inhibitor formulation by understanding the degradation mechanism of X60 pipeline steel in a CO_2-saturated chloride environment. Chitosan and CMC were chosen because of their unique electronic and molecular structures, since their anticorrosive properties as compounds are largely linked with their chemical makeup. Specifically, the β-(1-4)-linked D-glucosamine/N-acetyl-D-glucosamine and carboxymethyl-bound glucopyranyl moieties on chitosan and CMC, respectively, bear some O and N heteroatoms capable of adsorption at the surface of X60 steel, thereby forming a mass/charge barrier against further corrosive attack, hence inhibition (Figure 6). Apart from being multifunctional group compounds, chitosan and CMC are green, stable, benign, and biodegradable inhibitors.

Variations in Z values of the Nyquist curves correspond to the Bode and phase angle (θ) plots. Apart from the phase current (with respect to the applied potential) and the amplitude of the current being simultaneously measured, another advantage of using EIS for electrochemical surface probing of alternating current (AC) systems over a range of frequencies is that it aids in rationalizing the corrosion resistance mechanism of adhered films by using equivalent circuit models [63]. Equivalent circuit models provide an insight into the significance of the variation of impedance parameters from each response derived from the EIS spectra (Figures 9–11). In this study, it consisted of R_f and CPE $_f$ in parallel, representing the adsorbed species-forming films on the surface of the

X60 pipeline steel samples in the solution of the electrolyte with resistance (R_s); the charge transfer resistance (R_{ct}); and its double-layer constant-phase element component (CPE_{dl}), in parallel with the first set of components. In this study, the electrochemical equivalent circuit models presented in Figure 12 were used in fitting the impedance data in the absence and presence of chitosan, CMC, and the commercial inhibitor, with R_p calculated from Equation 4.1:

$$R_p = R_f + R_{ct} \tag{4.1}$$

CPE is mainly used in describing frequency-independent phase shift (θ) (see phase angle plots) between the applied potential and the corresponding current response, and to address double-layer inhomogeneities as well as electrode surface irregularities. While CPE is related to a non-ideal dielectric property of the film (expressed in Equation 4.2), its exact impedance component (Z_{CPE}) is defined in Equation 4.3 [64]:

$$CPE = r \cdot \varepsilon \cdot \varepsilon_o \, {}^{A}/_{d} \tag{4.2}$$

$$Z_{CPE} = Y_o(j\omega)^{-n} \tag{4.3}$$

$\varepsilon_o = Electrical\ Permittivity$
$\varepsilon = Film's\ Dielectric\ Constant$
$A = Exposed\ Area\ of\ Metal$
$d = Thickness\ of\ the\ film$
$r = Film\ Roughness\ Factor$
$Y_o = Pseudo\ Capacitance$
$\omega = Angular\ Frequency$

The choice of equivalent circuit models in this study is based on the respective contributions of every inhibitor; their physical meanings are denoted for each

representative circuit component. As presented in Figure 12, these models best fit the experimental impedance in the absence (a) and presence (b) of the inhibitors. In these circuit models, R_s denotes the resistance of the CO_2-saturated 3.5% NaCl electrolytic solution, and the capacitance of the film is associated with the dielectric properties of the oxide film that is generated. R_f denotes the resistance of the flow of ionic current due to the presence of corrosive ions and molecules of the electrolyte deep within the pores and cracks of the film. Close to the metal surface is another pseudo-layer; here, R_{ct} represents the charge transfer resistance, while a capacitance component (C_{dl}) describes the electrochemical double-layer's non-ideal properties at the metal/solution interface. The magnitude of R_{ct} is inversely proportional to the corrosion rate of the test substrate. A constant phase element is used to replace capacitance in order to account for the electrode's surface roughness and any inherent heterogeneities that may have occurred at the oxide layer and the inherent dispersive characteristics of time constants. From the electrical impedance of a CPE impedance (Z_{CPE}) which is defined in Equation 4.4, we may see that the capacitance values of the coatings, CPEc (Y_o), denote the water uptake ability of the film; a higher level of water uptake by the film means larger CPE values. Equation 4.4 also contains a component that defines the characteristic of the CPE, termed "CPE power (n)"; normally, the magnitude of this quantity ranges $-1 < n < 1$. CPE is resistive if $n = 0$; capacitive if $n = 1$ (positive); or inductive if $n = -1$. It can also be considered to be Warburg admittance if $n = 0.5$; "n" is also referred to as the "system homogeneity factor." The *n* values, as displayed in Table 5, reveal that the characteristic of CPE is capacitive, since it is positive. Table 5 lists the derived electrochemical parameters from the Nyquist plots (Figures 9–11) for X60 pipeline steel in the CO_2-

saturated 3.5% NaCl solution with and without different concentrations of chitosan, CMC, and the commercial inhibitor. The Nyquist curve semi-circle for 100 ppm chitosan appears to be wider than that of CMC at the same concentration, which denotes better metal protection in the presence of chitosan.

From the tabulated electrochemical data, the increase in the values of R_p at the electrode/electrolyte interface was found to increase with the concentration of chitosan and CMC. However, 75 ppm seems to be the optimum concentration of the commercial inhibitor for steel protection in this medium, where R_p drops for the highest concentration, indicating a saturation of the adsorbed film at the electrode surface. At this concentration, the adsorbed species must have saturated the electrode surface, and thus became porous due to the constant corrosive attack in the presence of the CO_2 gas. Again, the increase in the values of R_p with concentration of the inhibitors confirms corrosion inhibition. The higher values of R_p for the three inhibitors are in this order: Commercial inhibitor >> chitosan > CMC. Chitosan and CMC are showing good close protection abilities for X60 pipeline steel, and they are only single-component, water-soluble inhibitors. It is worth noting, however, that there was no exact trend in the variation of R_p with the concentration of inhibitors. A similar trend for the resistances for each inhibitor concentration was observed for CPE_{dl} (measured in $\mu F/cm^2$).

The reduction in the magnitude of capacitance at higher concentrations of the inhibitors may be attributed to the adsorption of intermediate species of these compounds on the surface of the steel substrate by mass transfer, thereby reducing the corrosion rate. The Bode modulus curves (Figures 9–11b) for all of the concentrations of inhibitors in this study exhibited a characteristic slanted |Z| shape at the medium-level frequencies

(between 1 and 10 Hz), and a slight change observed for the commercial inhibitor, stretching up to 0.1 Hz. Higher Z values are associated with higher corrosion resistance due to the presence of the inhibitor; in this study, chitosan recorded higher Z values compared to CMC for all of the concentrations. Z values up to 325, 270, 250, and 222 Ω cm^2 were recorded for 100, 75, 50, and 25 ppm chitosan, respectively, compared to equal concentrations of CMC (287, 274, 251, and 240 Ω cm^2) at 0.1 Hz, in that order.

The commercial inhibitor demonstrates superior inhibition, with Z values between 1,250 and 2,500 Ω cm^2 recorded at the same concentration as those of chitosan and CMC. The Bode phase angle curves (Figures 9–11c) reveal single broad maxima at 100 Hz for all concentrations of chitosan (and 25 and 100 ppm CMC only), unlike those of the commercial inhibitor observed at 10 Hz.

For the blank solution at the medium frequencies, there appeared to be some linearity in the curve, but with the gradient of the curves to less than unity, corresponding to $\theta < 90°$; this denotes the formation of a passive oxide layer with non-capacitive behavior in a diffusion-controlled corrosion process. At 100 Hz, values of θ (–70, –59, –80, and $–71^o$) were recorded for 100, 75, 50, and 25 ppm chitosan, respectively, while the Z maxima for 25 and 100 ppm CMC shifted to –65 and $–60^o$ at 100 Hz, respectively. This shift, compared to the blank solution, could be attributed to the adsorption of more of the CMC molecules on the metal surface. As the inhibitor molecules self-assembled on steel, a new loop was formed on the phase angle curve; this was distinct at 10 kHz for chitosan and the commercial inhibitor compared to CMC (for 50 and 75 ppm only) at 1 kHz.

Corrosion protection in this case depends on the concentration of active inhibitor molecules, as well as their solubility and diffusion rates as they approach the metal. Normally, phase angle plots are used to show the frequency-independent phase shift (θ) between the applied potential and its corresponding current response in EIS spectra; when θ ≈ 90°, the current passes through a capacitor, and the metal/electrolyte interface could be considered to be capacitive [64]. We can see in the phase diagrams (Figures 9–11c) that the inhibitor systems under study showed wide capacitive behavior, with θ close to 90^{o} for every concentration. This behavior is related to the extent of the uptake of water at the metal surface (Equation 4.5): molecules of the inhibitors may have reacted at the substrate with the surrounding Fe^{2+} ions, thereby forming a $[\mathrm{Fe}-\mathrm{Inh}]_{\mathrm{ads}}^{2+}$-type complex (Equations 4.6 and 4.7) [66].

$$Inh_{sol} + xH_2O_{ads} \rightarrow Inh_{ads} + xH_2O_{sol} \quad (4.5)$$

$$Fe \rightarrow Fe^{2+} + 2e^{-} \quad (4.6)$$

$$Fe^{2+} + Inh_{ads} \rightarrow [Fe - Inh]_{ads}^{2+} \quad (4.7)$$

At lower frequencies for each system, θ gradually drops, reaching 0° for all the inhibitors, except for chitosan. At lower frequencies, the most inhibiting concentrations of each system should have the lowest θ compared to the blank, hence reduced corrosion phenomena at the metal/solution interface [64, 65]. The trend in θ has shown that the performance of chitosan and CMC is similar on the X60 pipeline steel in CO_2-saturated saline solution.

Table 5: EIS parameters for the effect of concentration of inhibitors as it affects X60 pipeline steel corrosion in CO_2-saturated 3.5% NaCl solution.

Specimen	Concentration (ppm)	R_s (Ω cm^2)	CPE_f		R_f (Ω cm^2)	CPE_{dl}		R_{ct} (Ω cm^2)	$x^2 \times 10^{-3}$	R_p (Ω cm^2)	IE(%)
			C (μF/cm^2)	n_1		C (μF/cm^2)	n_2				
Blank	-	1.5	-	-	-	521	0.85	186.9	2.74	187	-
Chitosan	25	0.7	148	1.00	9.5	759	0.71	225.8	15.8	235	21
	50	0.7	175	1.00	26.7	704	0.73	240.6	18.2	267	30
	75	1.9	406	0.84	72.2	355	0.74	211.2	1.93	283	34
	100	1.0	103	1.00	5.2	723	0.67	331.7	8.59	337	45
CMC	25	1.0	228	0.93	40.4	363	0.79	226.8	5.44	267	28
	50	0.3	180	1.00	54.5	442	0.83	219.1	6.21	274	32
	75	0.5	190	1.00	91.6	573	0.84	186.8	6.41	278	33
	100	1.6	266	0.89	32.2	322	0.74	272.0	4.01	304	39
Commercial	25	5.9	155	0.64	12.4	118	0.82	1404	1.24	1416	87
	50	2.6	355	0.62	13.1	37	0.98	1494	1.04	1507	87
	75	3.2	23	0.80	19.7	169	0.78	2833	3.20	2853	93
	100	2.0	4	1.00	9.3	281	0.76	1601	2.76	1610	88

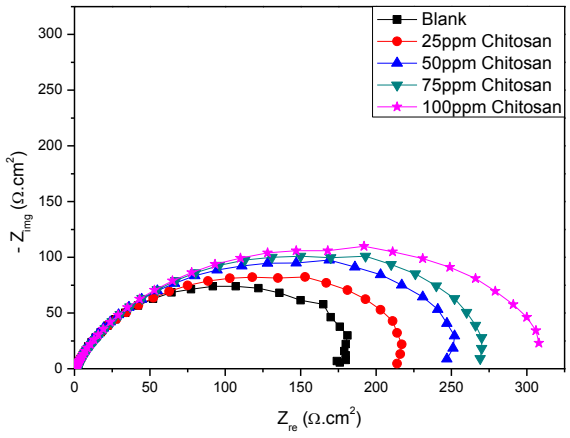

(a)

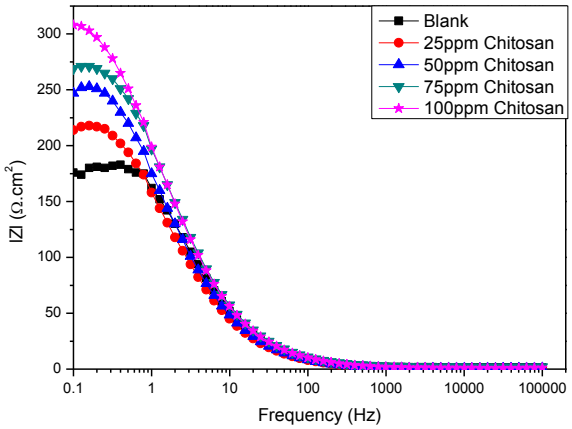

(b)

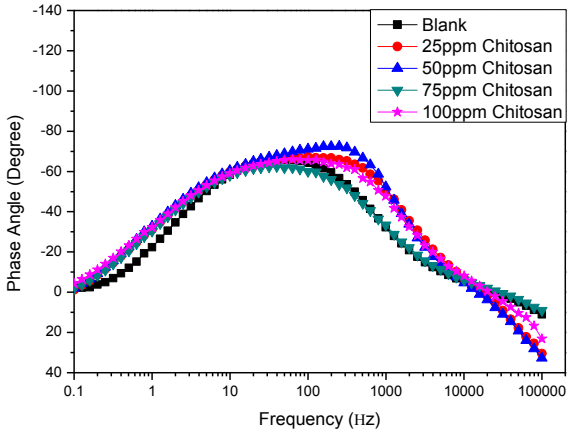

(c)

Figure 9: EIS spectra for the effect of concentration of chitosan as it affects X60 pipeline steel corrosion in CO_2-saturated 3.5% NaCl solution: (a) Nyquist, (b) Bode, and (c) Phase Angle.

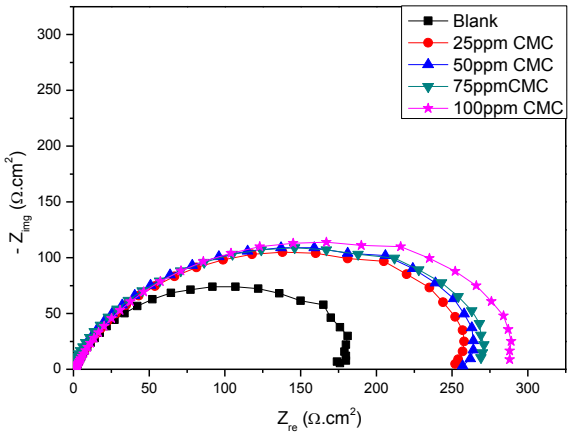

(a)

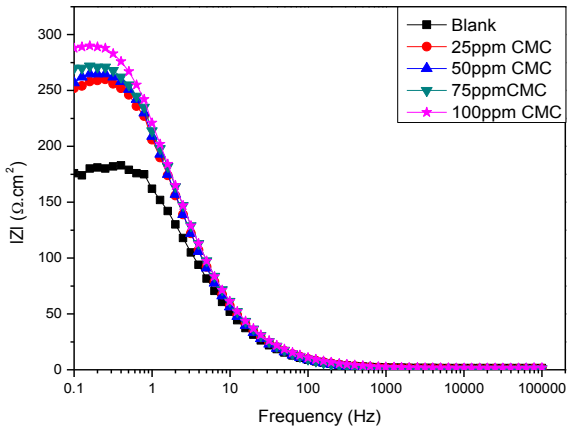

(b)

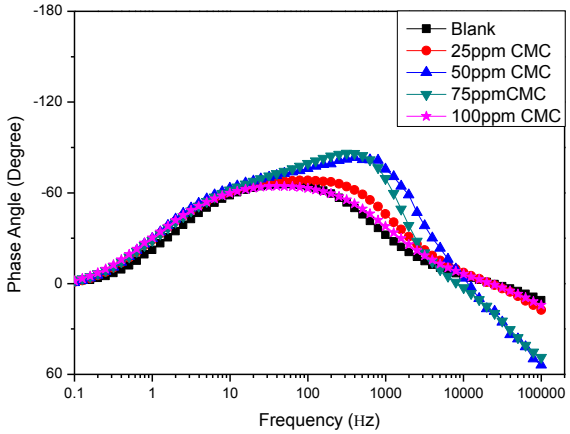

(c)

Figure 10: EIS spectra for the effect of concentration of CMC as it affects X60 pipeline steel corrosion in CO_2-saturated 3.5% NaCl solution: (a) Nyquist, (b) Bode, and (c) Phase Angle.

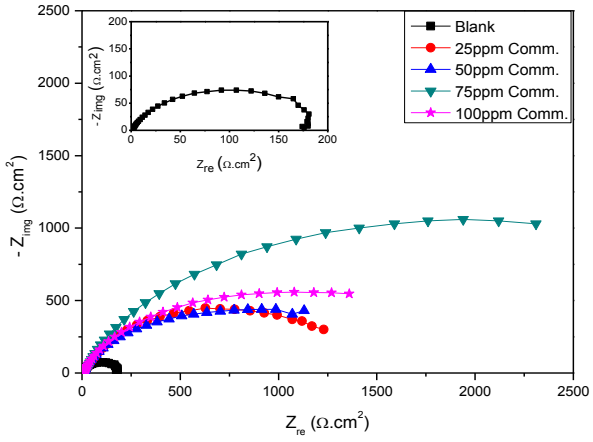

(a)

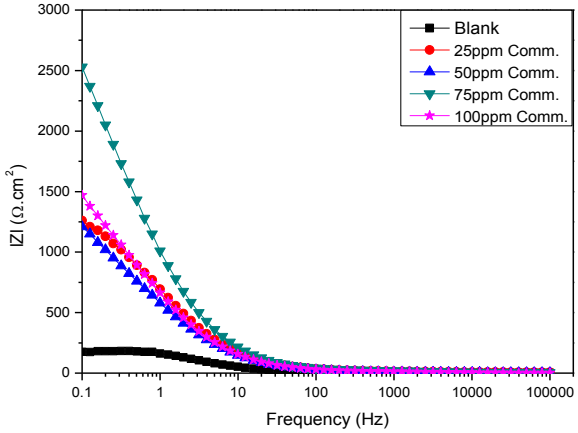

(b)

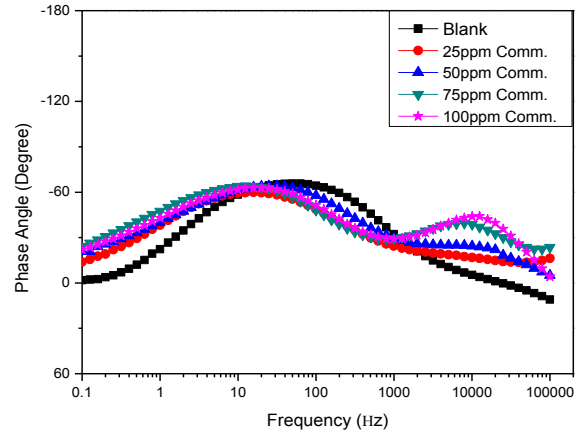

(c)

Figure 11: EIS spectra for the effect of concentration of the commercial inhibitor as it affects X60 pipeline steel corrosion in CO_2-saturated 3.5% NaCl solution: (a) Nyquist, (b) Bode, and (c) Phase Angle.

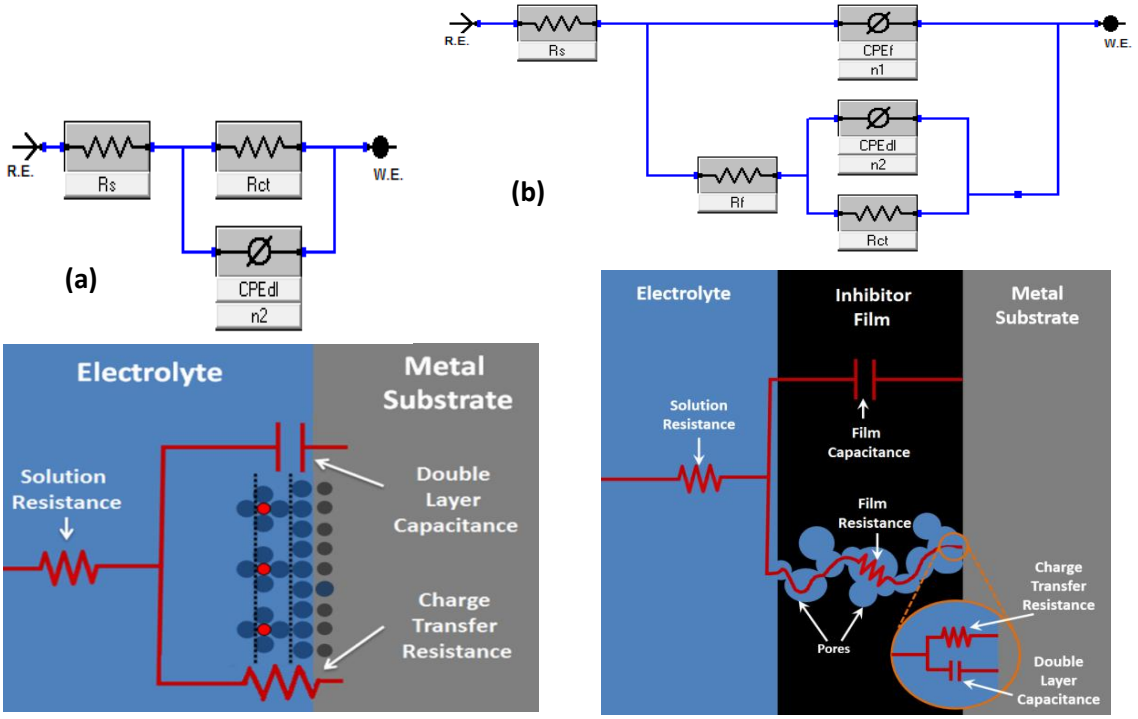

Figure 12 : Electrical equivalent circuit used to fit the impedance data: (a) simple Randel circuit for blank solution, and (b) circuit model used for the inhibited system [77].

4.1.2 PDP Results

The potentiodynamic polarization curves for the effect of concentration of chitosan, CMC, and the commercial inhibitor are presented in Figures 13, 14, and 15, respectively, for X60 pipeline steel in CO_2-saturated and static 3.5% NaCl solution. The curves show active anodic behavior, with the current intensity increasing as the potential is applied, without a distinctive transition to passivation within the potential range studied. The hydration of CO_2 to provide carbonic acid in the solution of the electrolyte follows Equation 4.8, and the cathodic reaction is the H^+ reduction enhanced by the carbonic acid dissociation in de-aerated electrolytes (Equations 4.9–4.11) [67]:

$$CO_2 + H_2O \rightarrow H_2CO_3 \tag{4.8}$$

$$H_2CO_3 \rightarrow H^+ + HCO_3^- \tag{4.9}$$

$$HCO_3^- \rightarrow H^+ + CO_3^{2-} \tag{4.10}$$

$$H^+ + e^- \rightarrow {}^1/_2\, H_2 \tag{4.11}$$

The curves for all of the concentrations of inhibitors studied, and for the blank solution, obey Tafel's behavior. Table 6 shows the values of corrosion current density (i_{corr}), corrosion potential (E_{corr}), and the cathodic (β_c) and anodic (β_a) Tafel slopes constants derived from the polarization curves. Compared to the blank solution, the values of i_{corr} decreased with the concentration of the three inhibitors; the commercial compound had the least values (meaning it was the most protective) for X60 pipeline steel in CO_2-saturated saline solution. The optimum concentration of the commercial inhibitor for steel protection in this medium seems to be 75 ppm, above which point the protective film

breaks (also called “steady state concentration”) and inhibition drops [68]. This assertion is also reflected in the Inhibition Efficiency (IE%) values. Higher concentrations of chitosan has better inhibited the steel surface; this could be attributed to the abundance of the amino-bearing glucosamine group in chitosan, which is capable of stable adsorption at the surface of X60 steel via its lone pairs of electrons. The current density values (37.2 and 39.8 $\mu A/cm^2$) were recorded for 100 and 75 ppm chitosan, respectively, compared to 37.9 and 41.0 $\mu A/cm^2$ for the same concentration range for CMC.

The values of IE% for this technique were calculated in the absence and presence of inhibitors using the magnitudes of corrosion current density (Equation 3.8). The highest values of corrosion inhibitor efficiency were recorded for 75 ppm commercial inhibitor (95%), 100 ppm chitosan (51%), and CMC (50%). The trend in IE% values follows that of i_{corr}, except that higher values are recorded for chitosan compared to CMC at 75 and 100 ppm; beyond this, IE% values are comparable to the commercial inhibitor. The values of E_{corr} do not change much in the presence of these inhibitors, making them a mixed-type system with E_{corr} approaching nobler values; this is also reflected in the redox Tafel slopes, measured in mV/ decade. Mixed-type inhibition systems are widely reported as possessing geometric blocking mechanisms on metal surfaces [68].

Table 6: Potentiodynamic polarization parameters for the effect of concentration as it affects X60 pipeline steel corrosion in CO_2-saturated 3.5% NaCl solution.

Specimen	Concentration (ppm)	$-E_{corr}$ *(mV/SCE)*	i_{corr} *($\mu A/cm^2$)*	β_a (mV/decade)	$-\beta_c$ (mV/decade)	CR (mpy)	IE(%)
Blank	-	729	76.50	45	252	26.42	-
Chitosan	25	686	66.70	32	221	23.04	13
	50	687	60.70	35	277	20.98	21
	75	687	39.80	30	125	13.73	48
	100	683	37.20	25	93	12.85	51
CMC	25	707	62.70	46	195	21.67	18
	50	699	55.30	35	148	19.10	28
	75	693	41.00	36	281	14.15	46
	100	692	37.90	28	97	13.09	50
Commercial	25	644	7.68	74	64	2.65	90
	50	631	6.38	86	154	2.20	92
	75	629	3.51	68	83	1.21	95
	100	627	5.62	82	95	1.94	93

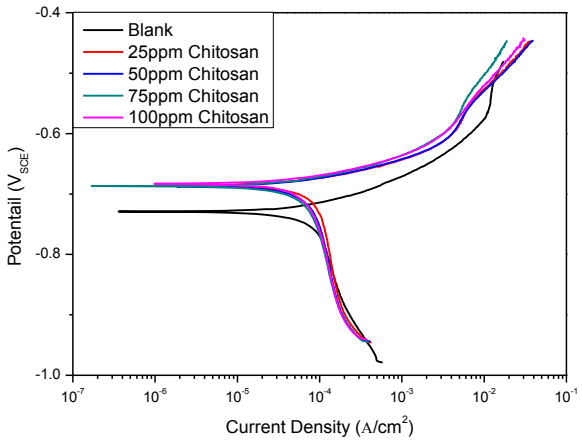

Figure 13: Potentiodynamic polarization curves for the effect of concentration of chitosan as it affects X60 pipeline steel corrosion in CO_2-saturated 3.5% NaCl solution.

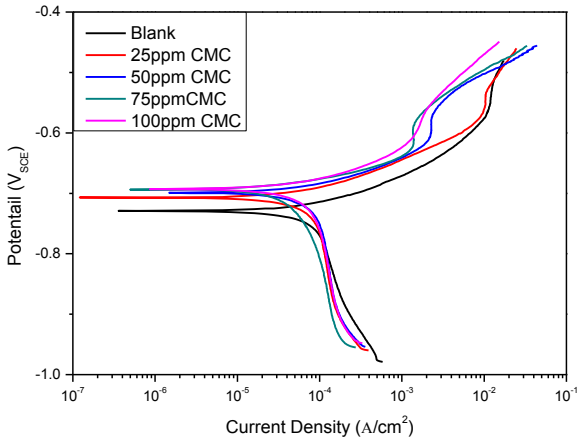

Figure 14: Potentiodynamic polarization curves for the effect of concentration of CMC as it affects X60 pipeline steel corrosion in CO_2-saturated 3.5% NaCl solution.

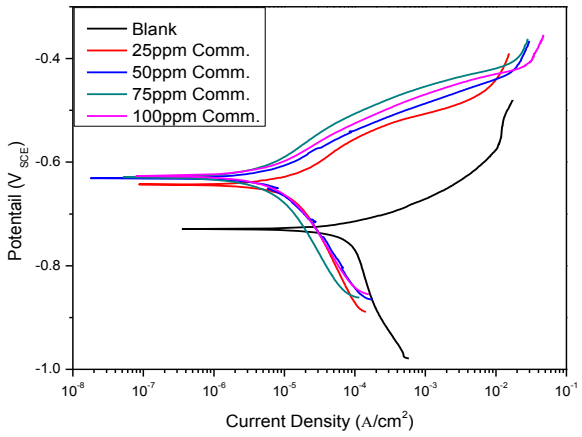

Figure 15: Potentiodynamic polarization curves for the effect of concentration of the commercial inhibitor as it affects X60 pipeline steel corrosion in CO_2-saturated 3.5% NaCl solution.

4.2 Effect of Temperature

4.2.1 EIS Results

Apart from the concentration of inhibiting species in the corrosive medium, corrosion inhibiting processes have also been found to be dependent upon temperature. In this study, the effect of varying the temperature has been investigated in CO_2-saturated saline solution for X60 pipeline steel using AC and DC electrochemical techniques. EIS technique has been deployed to correlate the corrosion rates of X60 pipeline steel substrate in the absence and presence of 100 ppm pure biopolymer compounds and the inhibitor formulation. The temperature dependence on X60 pipeline steel corrosion in CO_2-saturated saline solution was tested at 25°C, 40°C and 60°C for both the inhibited and uninhibited solutions. Figure 16 presents the EIS spectra in the presence and absence of 100 ppm chitosan at varying process temperatures (25°C–60°C). One-time constant Nyquist curves with full capacitive loops with and without chitosan and CMC are displayed in Figures 16(a) and 17(a), with wider curve diameters representing most protective systems. Similar spectra in the presence of the commercial inhibitor alone between 25°–60°C are shown in Figure 18: (a) Nyquist, (b) Bode, and (c) phase angle vs. frequency representations. Since the general shapes of the curves are maintained, this condition could be attributed to an unchanged corrosion mechanism at varying thermal conditions. For every inhibitor in this study, a reduced corrosion protection was determined for X60 pipeline steel in the CO_2-saturated 3.5% NaCl solution as the temperature increased, which is evident in the decrease in the Nyquist semi-circle diameters. Smaller semi-circle diameters, representing higher corrosion rates for steel, are revealed at 60°C than at the lower temperatures, irrespective of the inhibitor type. The Nyquist curve semi-circle for 100 ppm CMC appeared to be wider than that of chitosan at

the same concentration, which denotes superior metal protection in the presence of CMC at 60°C (although both compounds maintained relatively equal protective strength at 25°C).

The appropriate equivalent circuit models were used in fitting the impedance data and to provide insight into the significance of temperature variation with corrosion inhibition. The derived electrochemical parameters from the Nyquist plots for each inhibitor system after fitting the EIS data with these models (Figure 12) between 25°–60°C are displayed in Table 7. From the table, we can see that the values of R_p decreased at the electrode/electrolyte interface as the temperature increased. Compared to chitosan, CMC shows slightly higher values of R_p, showing better protection for X60 steel. The trend of charge transfer resistance values indicates that chitosan and CMC provided less protection compared to the commercial inhibitor. The effect of temperature on corrosion inhibition is more pronounced in the Bode plots (b), with a lowering of impedance (Z) of the interface at lower frequencies in the presence of the inhibitors compared to the blank solution. In the absence of the inhibitors, the X60 pipeline steel dissolved in the solution of the electrolyte at higher temperatures, evident in the lowering of the impedance values, but this reduced as the inhibitors were introduced.

The Bode modulus curves displayed in Figures 16–18b show the variation of Z values with frequency in the absence and presence of 100 ppm inhibitors at the temperatures under consideration. At 0.1 Hz, Z values up to 310, 95, and 70 Ω cm^2 were recorded for 100 pm chitosan at 25, 40, and 60°C, respectively, compared to the absence of this inhibitor concentration (175, 95, and 50 Ω cm^2) at the same temperature range. Similar variations of impedance data at the same frequency revealed slightly higher Z

values for CMC: 280, 125, and 80 Ω cm^2 at 25, 40, and 60°C, respectively; this denotes that CMC at higher temperatures proved to be a better candidate for a steel corrosion inhibitor compared to chitosan. Values for both chitosan and CMC are not comparable to those recorded for the commercial inhibitor, a multiple component inhibitor (1,500, 500, and 485 Ω cm^2) recorded at equal temperatures.

In all, the presence of the corrosion inhibitors demonstrated increased Z values compared to their absence for each temperature; the reduced Z values, which denote reduced corrosion protection, were observed at higher temperatures, which may be due to the desorption of inhibitor molecules from the metal surface in the saline electrolyte. Though there is no distinct evidence in the Bode modulus curves, new capacitive loops emerged from the Bode phase angle curves in the blank solution at 40 and 60°C at 10 kHz, which could be due to the formation of $FeCO_3$ scales on the steel substrate by charge transfer processes that occurred within the film/NaCl interface.

A similar feature was found in the Bode phase angle curves in the presence of 100 ppm commercial inhibitor between 25 and 60°C at the same frequency, with the θ magnitude increasing at this point (–50, –30, and –25° recorded at 25, 40, and 60°C, respectively) for the commercial inhibitor, compared to the maximum θ values at 25 and 60°C being relatively close (–58 and –60°, respectively). Generally, this feature could also be related to the accumulation of self-assembled inhibitor molecules forming compact films on the metal surface, which was detected at higher frequencies. A similar assertion could be attributed to the inhibiting systems at medium-level frequencies. The curves became more linear at higher temperatures (40 and 60°C) between 1 and 10 Hz, and the gradients of the curves at this position were less than unity, though greater for the

inhibiting systems compared to the uninhibiting system. The phase angle (θ) values gradually dropped to zero at 0.1 Hz, since |Z| magnitude attained constant magnitude in the absence and presence of the corrosion inhibitors.

Generally, an increase in the corrosion rates of metals in the presence of inhibitors at higher temperatures can be attributed to desorption of the inhibitor molecules from the metal surface. This behavior suggests physical adsorption of the inhibitors, since molecules of the inhibitor were displaced of adsorbed water molecules and became attached to the metal surface without chemical bonding (via van der Waal forces) [23,62]. Adsorption of the molecules of the inhibitors tended to reduce the X60 steel corrosion at 25°C; but at 40°C, the IE% values dropped due to molecular desorption and then subsequently rose again at 60°C. The percentage increase in the magnitude of IE% between 40° and 60°C for chitosan, CMC, and the commercial inhibitor were 89, 68, and 9%, respectively. The reason for this increment in the values of the corrosion inhibition efficiency at 60°C may be due to the change in the mechanism of inhibitor adsorption from physisorption to chemisorption may also account for the observed increase in inhibition efficiency while the temperature was raised from 40 to 60°C.

Table 7: EIS Parameters for the effect of temperature as it affects X60 pipeline steel corrosion in CO_2-saturated 3.5% NaCl solution in the presence and absence of chitosan, CMC, and the commercial inhibitor.

Specimen	Temp. (°C)	R_s (Ω cm^2)	CPE_f		R_f (Ω cm^2)	CPE_{dl}		R_{ct} (Ω cm^2)	$x^2 \times 10^{-3}$	R_p (Ω cm^2)	IE(%)
			C (μF/cm^2)	n_1		C (μF/cm^2)	n_2				
Blank	25	1.5	-	-	-	521	0.84	186.9	2.74	187	-
	40	2.7	-	-	-	818	0.81	94.8	0.87	95	-
	60	0.2	432	1.00	22.8	2175	0.85	24.6	7.79	47	-
Chitosan	25	1.0	103	1.00	5.2	723	0.66	331.7	8.59	337	45
	40	1.5	98	0.98	1.6	1282	0.64	96.7	2.79	98	4
	60	0.9	164	1.00	2.4	1322	0.68	70.3	6.65	73	35
CMC	25	1.6	266	0.89	32.2	322	0.74	272.0	4.01	304	39
	40	0.3	1.15	1.00	133	936	0.79	0.11	5.39	134	29
	60	0.9	178	0.98	8.5	1045	0.72	82.0	6.23	90	48
Commercial	25	2.0	4	1.00	9.3	281	0.76	1601.0	2.76	1610	88
	40	0.9	455	0.66	10.6	33	0.91	434.1	4.97	445	79
	60	1.9	3	1.00	2.3	466	0.71	376.8	0.59	379	87

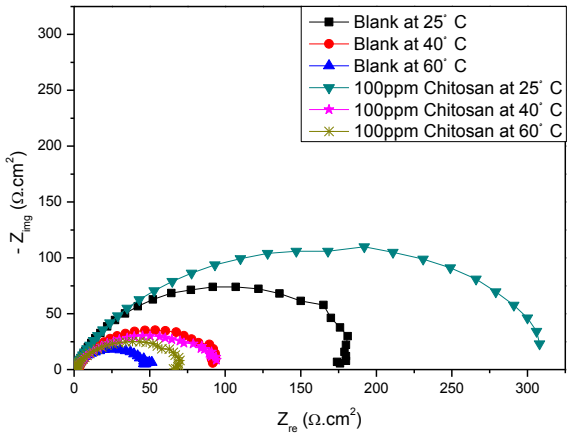

(a)

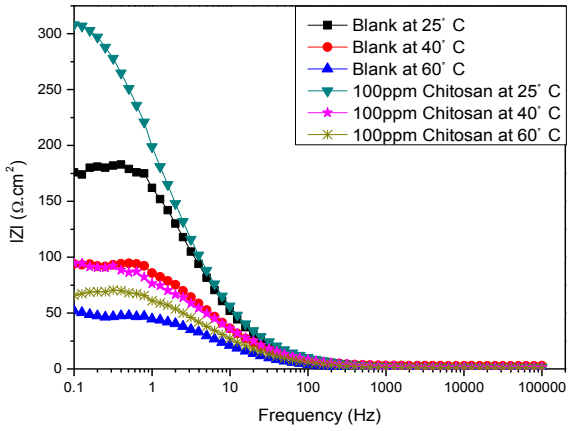

(b)

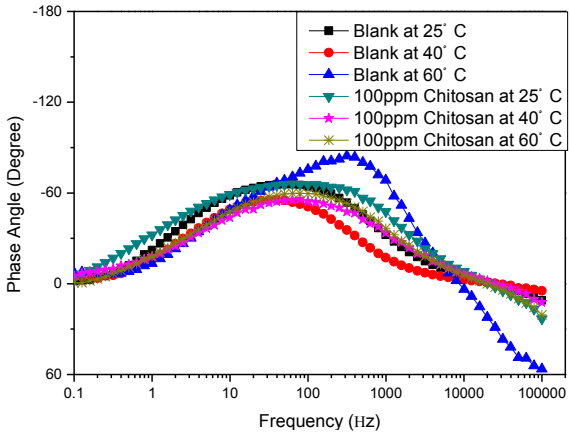

(c)

Figure 16: EIS spectra for the effect of temperature as it affects X60 pipeline steel corrosion in CO_2-saturated 3.5% NaCl solution in the presence and absence of 100 ppm chitosan: (a) Nyquist, (b) Bode, and (c) Phase Angle.

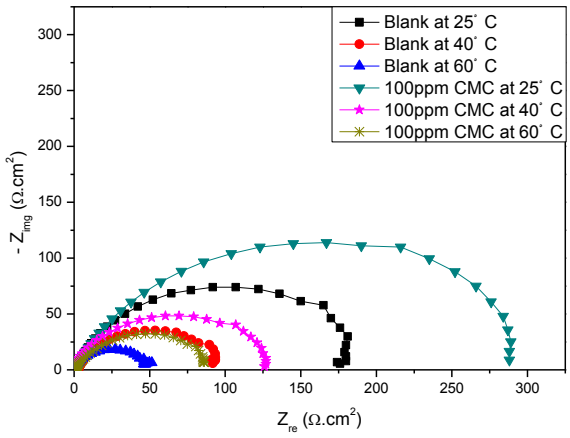

(a)

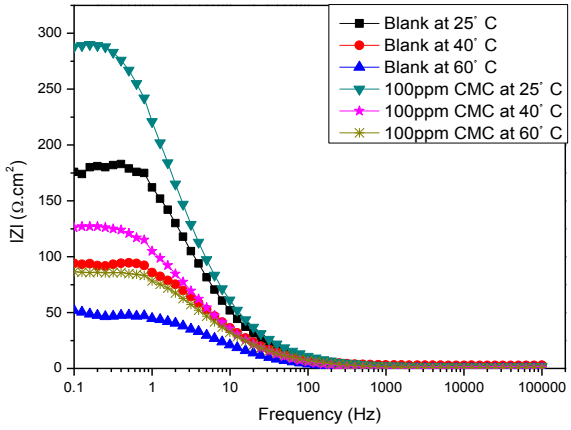

(b)

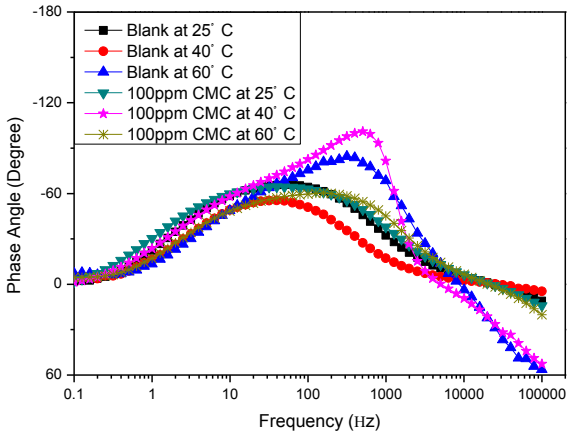

(c)

Figure 17: EIS spectra for the effect of temperature as it affects X60 pipeline steel corrosion in CO_2-saturated 3.5% NaCl solution in the presence and absence of 100 ppm CMC: (a) Nyquist, (b) Bode, and (c) Phase Angle.

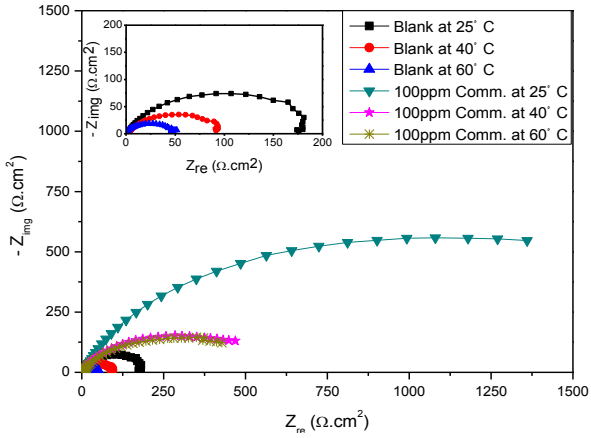

(a)

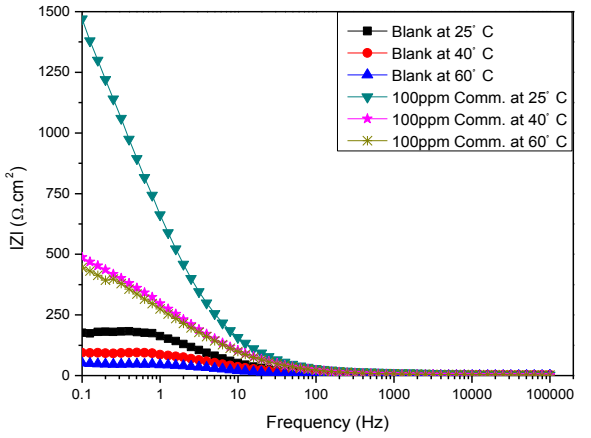

(b)

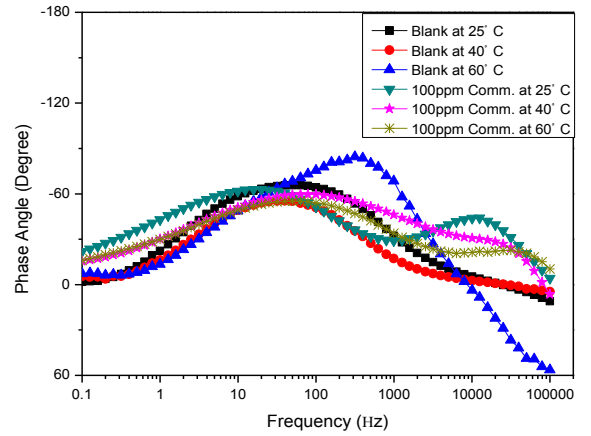

(c)

Figure 18: EIS spectra for the effect of temperature as it affects X60 pipeline steel corrosion in CO_2-saturated 3.5% NaCl solution in the presence and absence of 100 ppm commercial inhibitor: (a) Nyquist, (b) Bode, and (c) Phase Angle.

4.2.2 PDP Results

The effect of temperature was also studied for the corrosion of X60 pipeline steel in CO_2-saturated saline solution using the potentiodynamic polarization technique in the absence and presence of 100 ppm CMC, chitosan, and the commercial inhibitors between 25°–60°C. The respective potentiodynamic polarization curves are shown in Figures 19, 20, and 21, while the derived electrochemical parameters are listed in Table 8. The Tafel curves presented for the X60 pipeline steel in the solution of the test electrolyte (and within the thermal condition in this study) exhibit active dissolution without a distinctive transition to passivation within the potential range studied.

Since the values of i_{corr} can invariably give an idea of the corrosion rate for X60 pipeline steel in CO_2-saturated saline solution, the effect of temperature as it affects the corrosion rate of the substrate was evaluated from its magnitude. From the table, the values of i_{corr} were found to increase with temperature in the presence and absence of the corrosion inhibitors, with higher values recorded at 60°C. The values of i_{corr} may be observed to gradually increase with temperature, with higher magnitudes recorded in the absence of the inhibitors at 60°C. The shift in values of E_{corr} for the inhibitors relative to the blank seems more pronounced as the temperature rises, showing great influence of temperature variation on corrosion potential. From the results in Table 8, the minimum difference in these values is 46 mV for chitosan at 25°C, confirming the mixed-type inhibitor earlier proposed. Some researchers have argued that differences in E_{corr} to a magnitude greater than 85 mV for an inhibiting system relative to the blank solution implies a cathodic- or anodic-type system; otherwise, a mixed-type system is proposed [60,61]. The increase in corrosion rate with increased temperature in the

presence of the inhibitors in the CO_2-saturated saline electrolyte can be attributed to the inhibitor molecules desorption from the X60 pipeline steel surface at elevated temperatures. Since the formation of layers of $FeCO_3$ on the electrode surface is highly favored at higher temperatures (Equation 4.12), this surface phenomenon shifts the anodic and cathodic branches (mixed inhibitor systems) and further reduces the value of the corrosion current density. Reductions in the magnitude of current density are normally ascribed to the presence of more compact films on the surface of the electrode. Again, molecular adsorption inhibited the X60 steel dissolution at 25°C; as the temperature increased to 40°C, the IE% values dropped due to desorption of the adhered film. IE% values were found to increase again at 60°C for the single- and multi-component inhibitor systems and this could be attributed to the change in the mechanism of inhibitor adsorption from physisorption to chemisorption may also account for the observed increase in inhibition efficiency while the temperature was raised from 40 to 60°C.

Table 8: Potentiodynamic polarization parameters for the effect of temperature as it affects X60 pipeline steel corrosion in CO_2-saturated 3.5% NaCl solution in the presence and absence of chitosan, CMC, and the commercial inhibitor.

Specimen	Temperature (°C)	$-E_{corr}$ *(mV/SCE)*	i_{corr} *($\mu A/cm^2$)*	β_a (mV/decade)	$-\beta_c$ (mV/decade)	CR (mpy)	IE(%)
Blank	25	729	76.50	45	252	26.42	-
	40	709	120.00	21	136	41.45	-
	60	717	239.00	19	152	82.46	-
Chitosan	25	683	37.20	25	93	12.85	51
	40	699	113.00	29	105	39.17	6
	60	710	170.00	32	85	58.71	29
CMC	25	692	37.90	28	97	13.09	50
	40	692	95.80	24	300	33.10	20
	60	710	134.00	27	58	46.42	44
Commercial	25	627	5.62	82	95	1.94	93
	40	664	30.10	29	48	10.41	75
	60	664	32.50	18	23	11.23	86

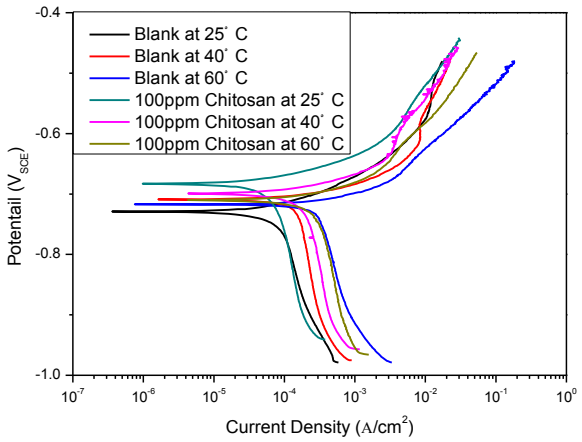

Figure 19: Potentiodynamic polarization curves for the effect of temperature as it affects X60 pipeline steel corrosion in CO_2-saturated 3.5% NaCl solution in the presence and absence of 100 ppm chitosan.

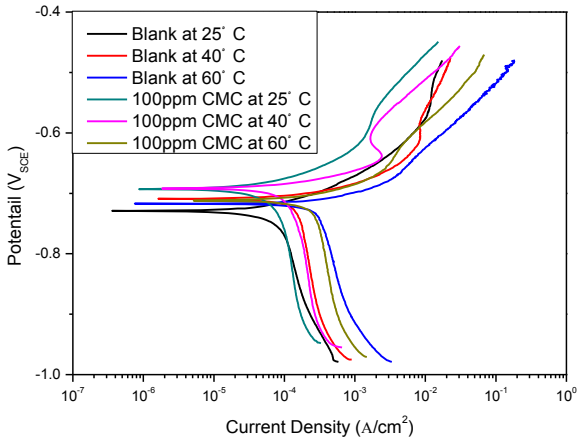

Figure 20: Potentiodynamic polarization curves for the effect of temperature as it affects X60 pipeline steel corrosion in CO_2-saturated 3.5% NaCl solution in the presence and absence of 100 ppm CMC.

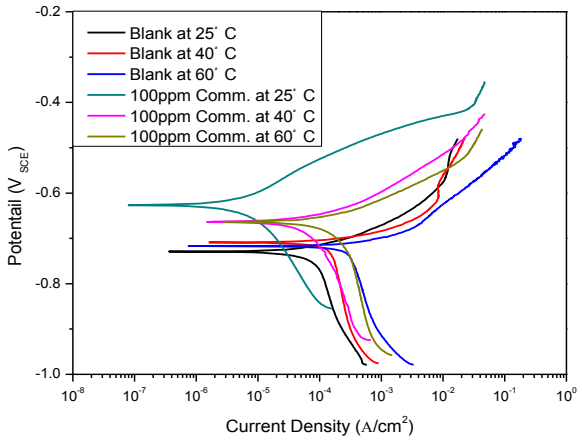

Figure 21: Potentiodynamic polarization curves for the effect of temperature as it affects X60 pipeline steel corrosion in CO_2-saturated 3.5% NaCl solution in the presence and absence of 100 ppm commercial inhibitor.

4.3 Effect of Exposure Time

4.3.1 EIS Results

In order to determine the effect of immersion time on the inhibitive action of the inhibitors for X60 pipeline steel in the CO_2-saturated saline solution, EIS measurements were performed between 1–24 hr at 25°C. Figures 22–24 display the changes in the Nyquist curves for the metal substrate with and without the addition of 100 ppm corrosion inhibitors (chitosan, CMC, and the commercial inhibitor). From the similar nature of the Nyquist plots, we can predict that the mechanism of protection of the test metal did not change in the prolonged exposure period to the CO_2-saturated saline electrolyte. The gradual increase in the diameter of the Nyquist curve after 12- and 24-hr exposure periods for chitosan indicates further protection of the steel substrate (Figure 22a). Similar curves were recorded for CMC and the commercial inhibitor between 1 and 24 hr. The Nyquist curve semi-circle for 100 ppm CMC appeared wider than that of chitosan at the same concentration, which denotes better metal protection in the presence of CMC after 24 hr immersion in the electrolyte solution, although there was a decrease in impedance value for CMC after this period (previously 400 Ω cm^2 at 0.1 Hz, compared to 200 Ω cm^2 recorded for chitosan).

The calculated electrochemical impedance parameters derived after fitting with appropriate equivalent circuit models are shown in Table 9. The curve diameter for the commercial inhibitor is wider compared to chitosan and CMC. For this experiment, it should be noted that CMC outperformed chitosan in showing better protection of the steel substrate upon prolonged immersion in the corrodent. This is evident in the improved R_p values at prolonged exposure times; 282 and 341 Ω cm^2 were recorded after 1- and 24-hr

exposure periods of X60 pipeline metal in the CO_2-saturated saline solution containing CMC. Similar exposure periods for chitosan recorded less R_p magnitude (175 and 254 Ω cm^2) for 100 ppm chitosan. The magnitude of X60 pipeline steel corrosion inhibition efficiency increased from 50% to 62% for CMC, which is greater than chitosan (19% to 34%), but much less than that obtained for the commercial inhibitor (88% to 94%). The increased corrosion protection for the X60 pipeline steel surface in the presence of the inhibitors in the CO_2-saturated saline electrolyte can be attributed to the increased adsorption of the inhibitor molecules on the steel surface during prolonged exposure periods. The higher magnitude of R_f for CMC compared to chitosan at the three immersion periods in this study could be attributed to the formation of more stable and compact inhibitor films by CMC, but with a porous passive oxide layer (denoting reduced R_{ct} values) close to the metal surface compared to chitosan. The inhibition efficiency of the inhibitors is thus dependent upon the exposure periods of the X60 pipeline steel in the CO_2-saturated saline solution containing the inhibitors. The increased inhibition efficiency with longer exposure durations also reflects a strong molecular adsorption, and more protective film on the steel/electrolyte interface. The decrease in corrosion inhibition efficiency for CMC observed after 24 hr compared to chitosan could be attributable to the formation of surface pitting upon prolonged immersion in the electrolyte solution. (This may be seen in the SEM micrographs in Section 4.5.)

The Bode modulus plots (Figures 22–24b) reveal remarkable increases in Z values with immersion time in the presence of the electrolyte due to molecular adsorption, since the time required for metal surface film adhesion increases with the exposure period. Z values at 0.1 Hz of up to 155, 200, and 230 Ω cm^2 were recorded in

the presence of 100 ppm chitosan, as compared to 275, 400, and 325 Ω cm^2 recorded at 1, 12, and 24 hr, respectively. Increases in Z values with frequency is dependent upon the immersion period; for both single and multiple component inhibitor systems, the lowest Z values were observed after exposure of the metal substrate in the first hour. Z values at 0.1 Hz of 2,250; 1,750; and 600 Ω cm^2 were recorded for 100 ppm commercial inhibitor at 1, 12, and 24 hr, respectively.

The Bode modulus curves showed increases in Z values at higher frequencies with immersion periods due to the formation of a more compact inhibitor film of the metal surface. There was also linearity in the curves between 1 and 10 Hz, though the magnitudes of the slopes were greater for the inhibitors compared to the blank solution for every immersion period. In Figures 22–24c, higher θ values were recorded for uninhibited solutions than those in the presence of chitosan and CMC between 10 and 1,000 Hz; the formation of new loops at 10 KHz for 100 ppm commercial inhibitor after prolonged immersion periods could be linked with multiple adsorption and subsequent retardation of the passage of corrosive ions.

Table 9: EIS parameters for the effect of immersion period as it affects X60 pipeline steel corrosion in CO_2-saturated 3.5% NaCl solution in the presence and absence of chitosan, CMC, and the commercial inhibitor.

Specimen	Time Duration (hours)	R_s (Ω cm^2)	CPE_f		R_f (Ω cm^2)	CPE_{dl}		R_{ct} (Ω cm^2)	$x^2 \times 10^{-3}$	R_p (Ω cm^2)	IE(%)
			C (μF/cm^2)	n_1		C (μF/cm^2)	n_2				
Blank	1	0.6	203	1.00	26.1	1107	0.76	115.0	3.91	141	-
	12	0.2	339	1.00	18.2	1349	0.81	140.6	11.5	159	-
	24	2.8	1091	0.77	23.4	694	0.84	144.4	2.08	168	-
Chitosan	1	1.8	70	1.00	2.9	969	0.63	172.3	2.18	175	19
	12	2.2	87	1.00	1.9	980	0.66	216.1	1.05	218	27
	24	2.4	82	1.00	2.4	754	0.71	251.8	1.45	254	34
CMC	1	4.6	474	0.78	217.8	505	1.00	64.6	1.72	282	50
	12	4.1	436	0.77	331.6	946	1.00	90.8	2.18	422	62
	24	4.3	573	0.77	289.9	2221	1.00	51.5	1.81	341	51
Commercial	1	15.2	296	0.76	610.0	2472	0.67	552.3	2.66	1162	88
	12	3.1	40	0.81	48.2	209	0.67	2136.0	0.69	2184	93
	24	6.4	18	0.82	61.9	154	0.67	2681.0	0.54	2743	94

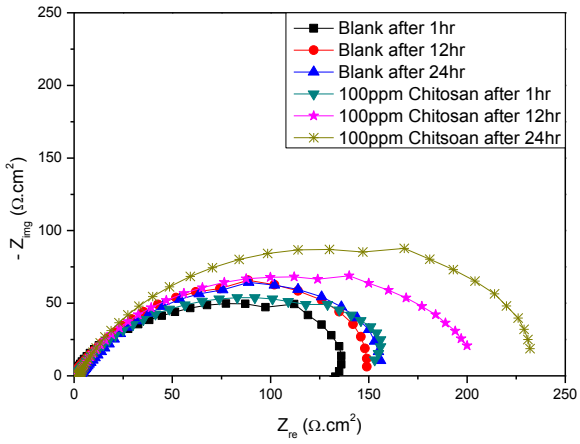

(a)

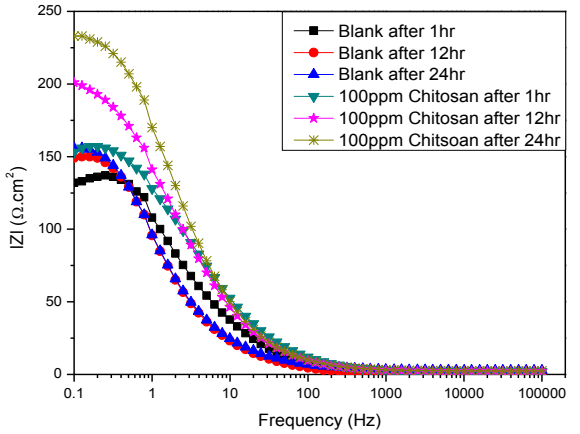

(b)

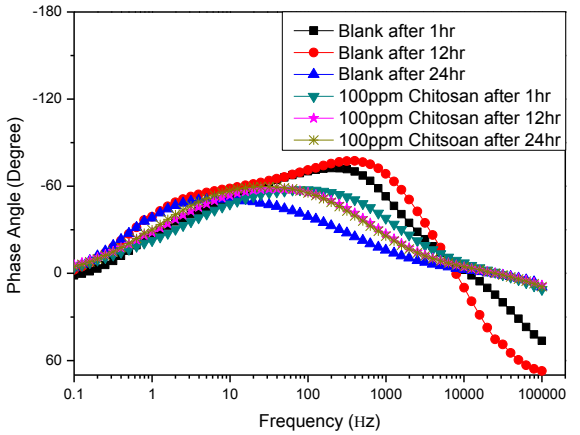

(c)

Figure 22: EIS spectra for the effect of immersion period as it affects X60 pipeline steel corrosion in CO_2-saturated 3.5% NaCl solution in the presence and absence of 100 ppm chitosan: (a) Nyquist, (b) Bode, and (c) Phase Angle.

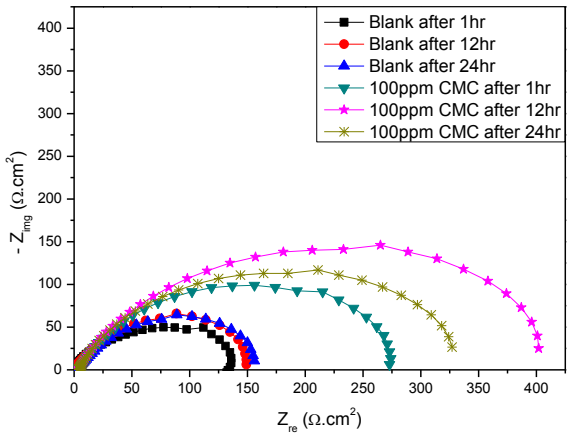

(a)

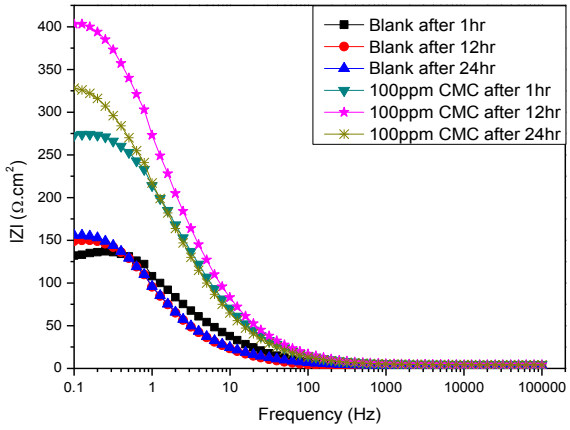

(b)

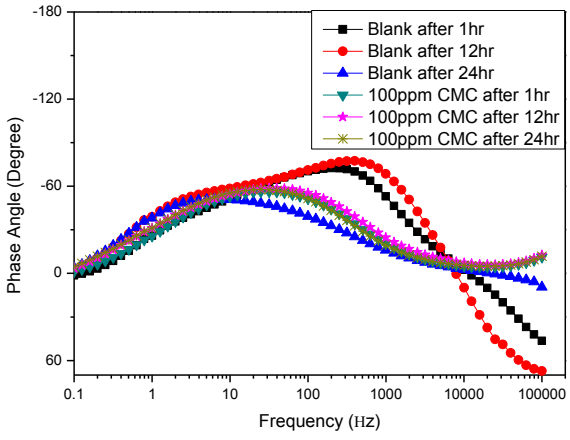

(c)

Figure 23: EIS spectra for the effect of immersion period as it affects X60 pipeline steel corrosion in CO_2-saturated 3.5% NaCl solution in the presence and absence of 100 ppm CMC: (a) Nyquist, (b) Bode, and (c) Phase Angle.

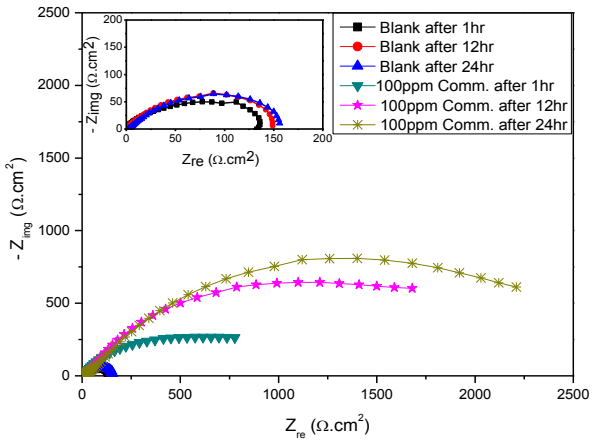

(a)

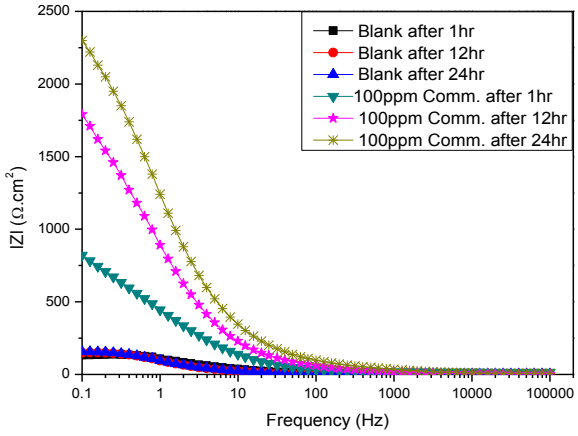

(b)

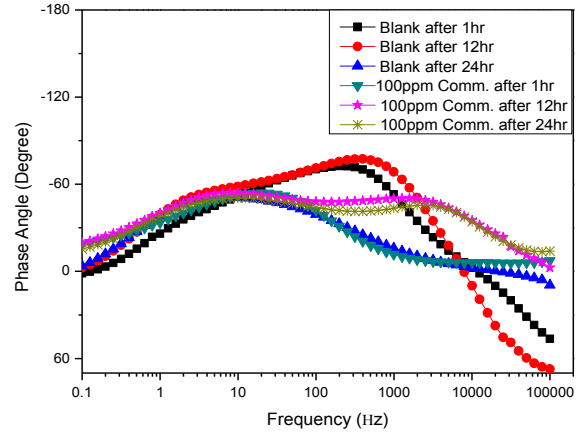

(c)

Figure 24: EIS spectra for the effect of immersion period as it affects X60 pipeline steel corrosion in CO_2-saturated 3.5% NaCl solution in the presence and absence of 100 ppm commercial inhibitor: (a) Nyquist, (b) Bode, and (c) Phase Angle.

4.4 Effect of Rotational Speed

4.4.1 EIS Results

Most corrosion inhibition studies for metal corrosion are focused on static conditions, with the search for the optimal concentration to which a particular compound (or group of compounds) can inhibit corrosion in a particular medium [68]. Static conditions are limited in nature, however, and few studies have studied the effect of flow conditions as it affects the rate of formation of protective films at the metal/electrolyte interface relative to the speed of working electrode rotation [69]. In this study, the inhibitive performance of chitosan, CMC, and the commercial inhibitor for X60 pipeline metal in the CO_2-saturated saline solution under dynamic conditions was investigated at 1,000 and 1,500 rpm using a rotating cylinder electrode (RCE) at 25°C with the setup shown in Figure 7. Figures 25–27 present the impedance spectra in (a) Nyquist, (b) Bode modulus, and (c) phase angle formats in the presence and absence of 100ppm chitosan, CMC, and the commercial inhibitor, respectively. The shapes of the Nyquist curves are similar, which is an indication of an unchanged mechanism of metal dissolution in the corrosive medium in the absence and presence of inhibitors as the speed of the RCE changes. Generally, in uninhibited solutions, the corrosion rate of metal substrates should increase with increasing rotational speed; this has been confirmed for X60 pipeline metal in the blank CO_2-saturated saline solution [68]. Increases in the diameter of the Nyquist plots may be observed for the blank solution at 1,000 rpm compared to 1,500 rpm. In the presence of an inhibitor, however, an increase in rotational speed implies that more inhibitor molecules will reach the metal surface to form a protective film, thereby improving corrosion inhibition. At low rotational speeds, the reduced mass transport of the inhibitor molecules at the metal surface in turn reduces the wall shear stress, thereby

separating the layers of adsorbed protective films at the metal/electrolyte interface; hence, there is inhibition reduction [68,69].

In the present study, corrosion inhibition efficiency was found to increase with increases in the rotational speed for the commercial inhibitor and CMC. Table 10 presents the derived electrochemical parameters after fitting the impedance data with the appropriate equivalent circuit models for X60 pipeline steel in the CO_2-saturated 3.5% NaCl solution in the absence and presence of 100 ppm chitosan, CMC, and the commercial inhibitor at 1,000 and 1,500 rpm. From the electrochemical data in Table 10, the gradual decrease in CPE_{dl} values with increased rotational speeds for each inhibitor system provides evidence of corrosion inhibition at higher speeds of rotation. Higher CPE_{dl} values were obtained in the absence of the inhibitors, with magnitudes of 1,262 and 1,602 μF/cm^2 recorded at 1,000 and 1,500 rpm, respectively, for the blank solution. As expected for R_p at higher rotational speeds, increased R_p values were recorded for 1,500 rpm only for CMC and the commercial inhibitor; the reason for this electrochemical behavior of chitosan is not entirely clear. At this rotational speed, 82 Ω cm^2 (the lowest R_p value in this study) was recorded for the blank CO_2-saturated 3.5% NaCl solution. The trend in R_p values therefore proves that for the blank uninhibited solutions, the rate of metal substrate dissolution increases with rotational speed [68]. The enhanced corrosion rate observed for chitosan suggests, however, that no protective inhibitor-adsorbed film was formed. The trend in IE values suggests that CMC is a better corrosion inhibitor for X60 pipeline steel under the dynamic condition.

Except in the presence of chitosan, the presence of every other inhibitor system, independent of rotational speed, increased the extent of corrosion protection. The Z

values in Figures 25–27b for the blank saline electrolyte appear to be higher compared to the presence of 100 ppm chitosan at 1,000 and 1,500 rpm for the range of frequency under consideration, which could be attributable to the molecular desorption of chitosan from the metal surface at higher rotational speeds. Reduced Z values compared to the uninhibited solution corresponded to more negative θ values in the Bode phase angle curves at lower frequencies.

A similar assertion could be proposed at higher rotational speeds for both single and multiple component systems. At 0.2 Hz, the Z magnitudes up to 80 and 70 Ω cm^2 were recorded at 1,000 and 1,500 rpm, respectively, compared to the blank solution (120 and 85 Ω cm^2). At the same frequency for CMC, the values of 113 and 100 Ω cm^2 were recorded at the same rotational speed. The Bode phase angle curves (in Figures 24–26c) for chitosan and CMC revealed the highest θ values at 20 Hz with single maxima and in the presence of the inhibitors compared to the blank solutions, independent of the speed. Only the θ curves for the commercial inhibitor possessed maxima at a different frequency from the blank solution, with –70 and –69^o recorded for this inhibitor at 1,000 and 1,500 rpm at 10 kHz, respectively. This provides evidence of the formation of protective films by diffusion at higher rotational speeds; it may also be attributable to the charge-transfer phenomenon, since more inhibitor molecules were brought to the charged metal surface.

Table 10: EIS parameters for the effect of rotational speed as it affects X60 pipeline steel corrosion in CO_2-saturated 3.5% NaCl solution in the presence and absence of chitosan, CMC, and the commercial inhibitor.

Specimen	Rotational Speed (rpm)	R_s (Ω cm^2)	CPE_f		R_f (Ω cm^2)	CPE_{dl}		R_{ct} (Ω cm^2)	$x^2 \times 10^{-3}$	R_p (Ω cm^2)	IE(%)
			C (μF/cm^2)	n_1		C (μF/cm^2)	n_2				
Blank	1,000	2.3	-	-	-	1,262	0.8346	129.0	5.88	129	-
	1,500	1.2	-	-	-	1,602	0.8338	82.2	3.77	82	-
Chitosan	1,000	1.4	796	0.8682	3.5	1,783	0.6358	73.9	0.44	77	-67
	1,500	1.6	547	0.9314	2.0	2,575	0.6524	68.6	0.46	71	-16
CMC	1,000	1.7	220	1.00	1.6	1,776	0.6650	108.6	2.35	110	-17
	1,500	1.3	163	1.00	1.1	1,672	0.6556	123.5	0.42	125	34
Commercial	1,000	1.5	4	0.9430	66.3	496	0.4259	699.9	0.15	766	83
	1,500	1.6	3	0.9425	65.0	238	0.4555	951.0	0.13	1,016	92

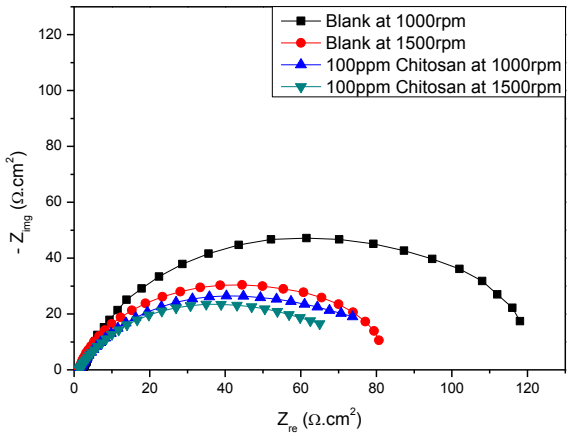

(a)

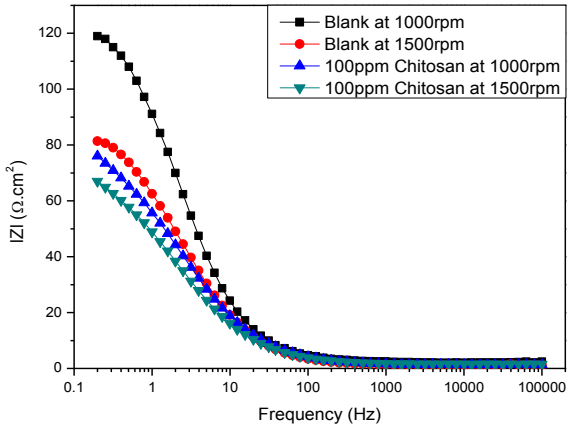

(b)

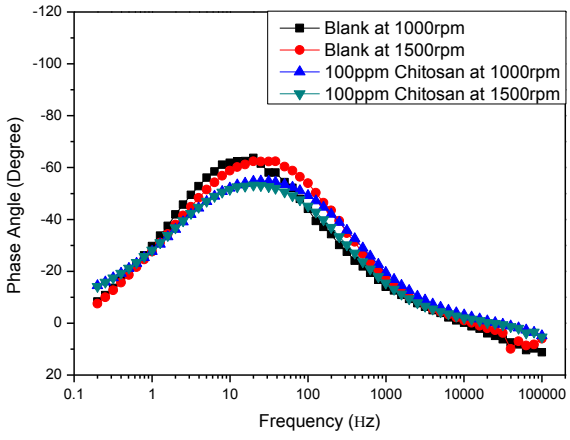

(c)

Figure 25: EIS spectra for the effect of rotational speed as it affects X60 pipeline steel corrosion in CO_2-saturated 3.5% NaCl solution in the presence and absence of 100 ppm chitosan: (a) Nyquist, (b) Bode, and (c) Phase Angle.

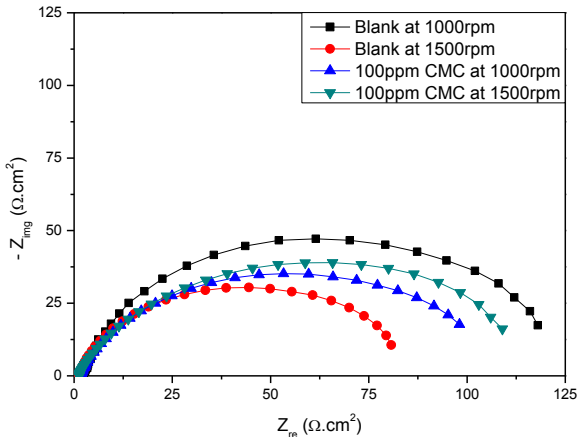

(a)

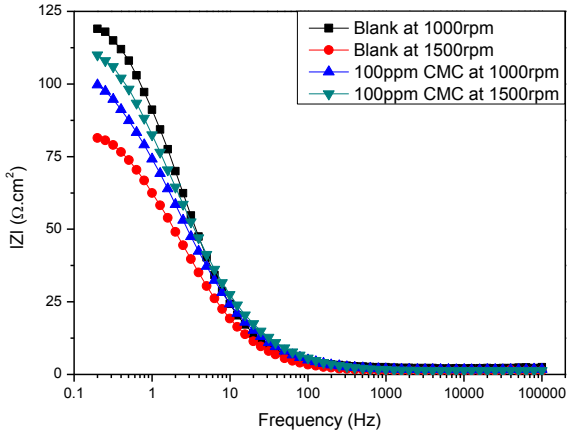

(b)

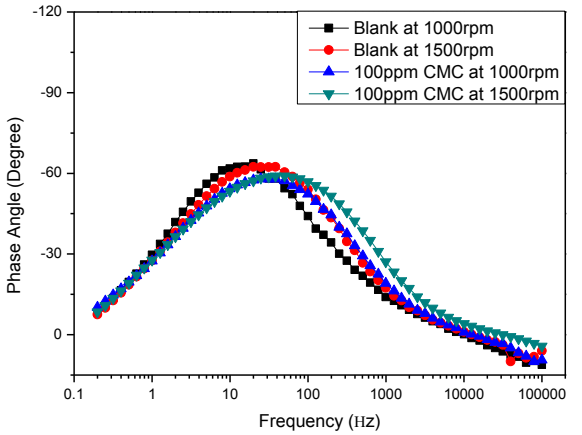

(c)

Figure 26: EIS spectra for the effect of rotational speed as it affects X60 pipeline steel corrosion in CO_2-saturated 3.5% NaCl solution in the presence and absence of 100 ppm CMC: (a) Nyquist, (b) Bode, and (c) Phase Angle.

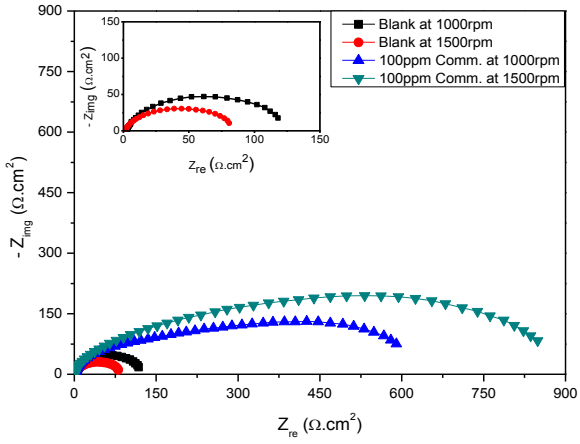

(a)

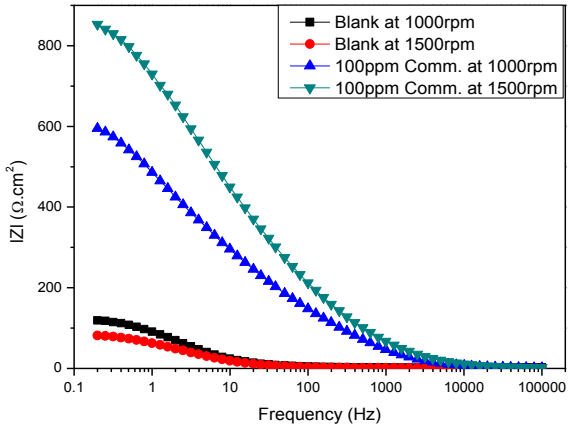

(b)

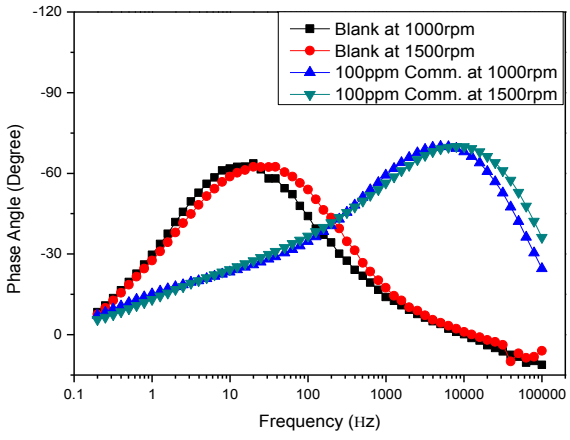

(c)

Figure 27: EIS spectra for the effect of rotational speed as it affects X60 pipeline steel corrosion in CO_2-saturated 3.5% NaCl solution in the presence and absence of 100 ppm commercial inhibitor: (a) Nyquist, (b) Bode, and (c) Phase Angle.

4.4.2 PDP Results

The variation in transportation modes of the surface-active species and the formation-destruction processes of protective films at the metal/solution interfaces are only a few of the important hydrodynamic factors that influence electrochemical measurement [70]. The effect of working electrode rotation speed was also studied for the corrosion of X60 pipeline steel in CO_2-saturated saline solution, using the potentiodynamic polarization technique in the absence and presence of 100 ppm single-component inhibitor compounds and the commercial inhibitor formulation at 1,000 and 1,500 rpm. The goal was to study the kinetics of redox reaction associated with hydrodynamics in the metal corrosion process. Figures 28–30 show the Tafel curves for 100 ppm chitosan, CMC, and the commercial inhibitor, respectively, for X60 steel investigated at different rotational speeds. The derived electrochemical parameters are presented in Table 11. The presented Tafel curves (those that are within the range of potential investigated in this study) show that the steel samples underwent active dissolution without distinctive transition to passivation for both rotational speeds. In the presence of inhibitors, the cathodic and anodic current shifted to regions of lower current density. As obtained in the EIS results, CMC inhibitor shows reduction in i_{corr} values with increased speed of rotation—thus affirming that improved protection associated with increased rotational speed, since more compact films are formed from molecules of the inhibitor that are brought to the metal surface by convection.

Apart from diffusion, increased corrosion protection at higher rotational speeds may be attributable to the phenomenon of charge-transfer, since molecules of the inhibitors are brought to the charged metal surface faster. The corrosion rates of X60

pipeline steel in CO_2-saturated saline solution was lower for CMC compared to chitosan, with a higher value (24.13 mpy) recorded for chitosan at 1,500 rpm. A corrosion rate of 2.43 mpy for the commercial inhibitor was obtained at the highest speed of rotation studied; this value is one order of magnitude less than CMC. A similar trend in the values of corrosion current density (i_{corr}), which is normally correlated with corrosion rate, reveals that, compared to chitosan, CMC offers better corrosion protection for X60 steel at 1,500 rpm. The magnitude of i_{corr} recorded for CMC (134 μA/cm^2) is lower than that of chitosan (158 μA/cm^2) at 1,000 rpm. Increased rotational speed correspondingly decreased the magnitude of i_{corr} for the inhibitor systems, except for chitosan. The lowest values for i_{corr} were recorded for the commercial inhibitor. The E_{corr} values did not significantly vary for any inhibitor system as the rotational speed increased (again, a mixed-type system is proposed). From the results obtained in this study, the corrosion inhibition performance of chitosan and CMC can be improved by increasing their concentration, and constituting a formulation to include additives such as enhancer, surfactant, and wetting agents. The significance of the electrochemical results produced by the Tafel experiment is in line with the EIS test.

Table 11: Potentiodynamic polarization parameters for the effect of rotational speed as it affects X60 pipeline steel corrosion in CO_2-saturated 3.5% NaCl solution in the presence and absence of chitosan, CMC, and the commercial inhibitor.

Specimen	Rotational Speed (rpm)	$-E_{corr}$ *(mV/SCE)*	i_{corr} *($\mu A/cm^2$)*	β_a (mV/decade)	$-\beta_c$ (mV/decade)	CR (mpy)	IE (%)
Blank	1,000	717	116.00	52	189	16.94	-
	1,500	715	152.00	43	164	22.05	-
Chitosan	1,000	704	158.00	73	297	22.96	-36
	1,500	703	166.00	70	223	24.13	-9
CMC	1,000	711	134.00	61	242	19.53	-16
	1,500	707	127.00	53	263	18.41	16
Commercial	1,000	729	32.40	143	218	4.72	72
	1,500	712	16.70	89	89	2.43	89

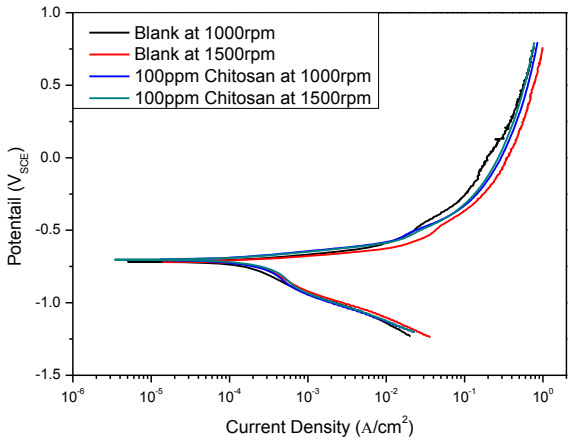

Figure 28: Potentiodynamic polarization curves for the effect of rotational speed as it affects X60 pipeline steel corrosion in CO_2-saturated 3.5% NaCl solution in the presence and absence of 100 ppm chitosan.

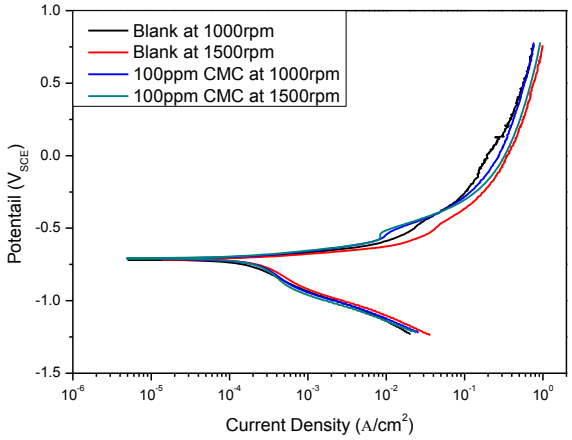

Figure 29: Potentiodynamic polarization curves for the effect of rotational speed as it affects X60 pipeline steel corrosion in CO_2-saturated 3.5% NaCl solution in the presence and absence of 100 ppm CMC.

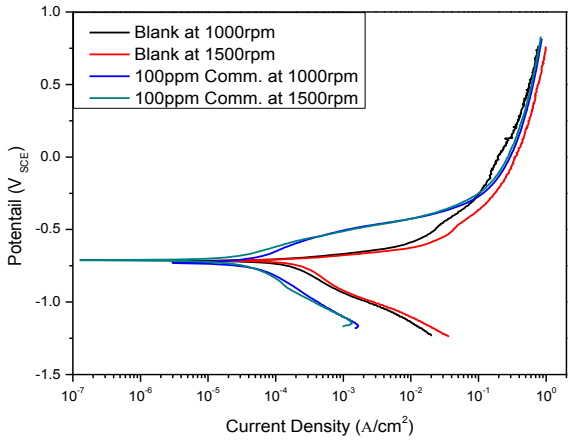

Figure 30: Potentiodynamic polarization curves for the effect of rotational speed as it affects X60 pipeline steel corrosion in CO_2-saturated 3.5% NaCl solution in the presence and absence of 100 ppm commercial inhibitor.

4.5 Metal Surface Characterization

The surface morphological examinations of the exposed steel specimens in uninhibited CO_2-saturated saline, and inhibited solutions containing pure biopolymers as corrosion inhibitor compounds and a commercially available corrosion inhibitor, were evaluated using a JEOL JSM-6610 LV scanning electron microscope. Figure 31 shows SEM images of the exposed X60 steel in CO_2-saturated saline solution in the absence and presence of 100 ppm of each inhibitor at room temperature after 24 hr immersion. The steel substrate in the uninhibited blank solution showed a severely corroded surface, with a very large corrosion product mass due to uncontrolled dissolution, as well as the other degradation caused by the presence of carbonic acid in the solution of the electrolyte (Figure 31a). While the steel substrate showed relatively uniform corrosion in the presence of chitosan, there seemed to be evidence of localized attack on the coupon in 100 ppm CMC. Generally, the presence of all of the corrosion inhibitors shows visible reduction in the corrosion of X60 pipeline steel, to a large extent due to the adsorption of molecules and the subsequent formation of protective layers on the metal surface [59,60]. The commercial inhibitor continued to show superior corrosion protection. This is evident in the clear SEM micrograph of the steel coupon in the solution of the electrolyte containing this inhibitor formulation—with few mold-like corrosion products and scales as continuous surface features. Chitosan and CMC have also shown good corrosion protection in CO_2-saturated saline solution for the same metal substrate. Chitosan and CMC with concentrations as low as 100 ppm could serve as green additives for superior protective inhibitor formulations for industrial pipeline steel applications, and are safer for the environment than the commercial inhibitor.

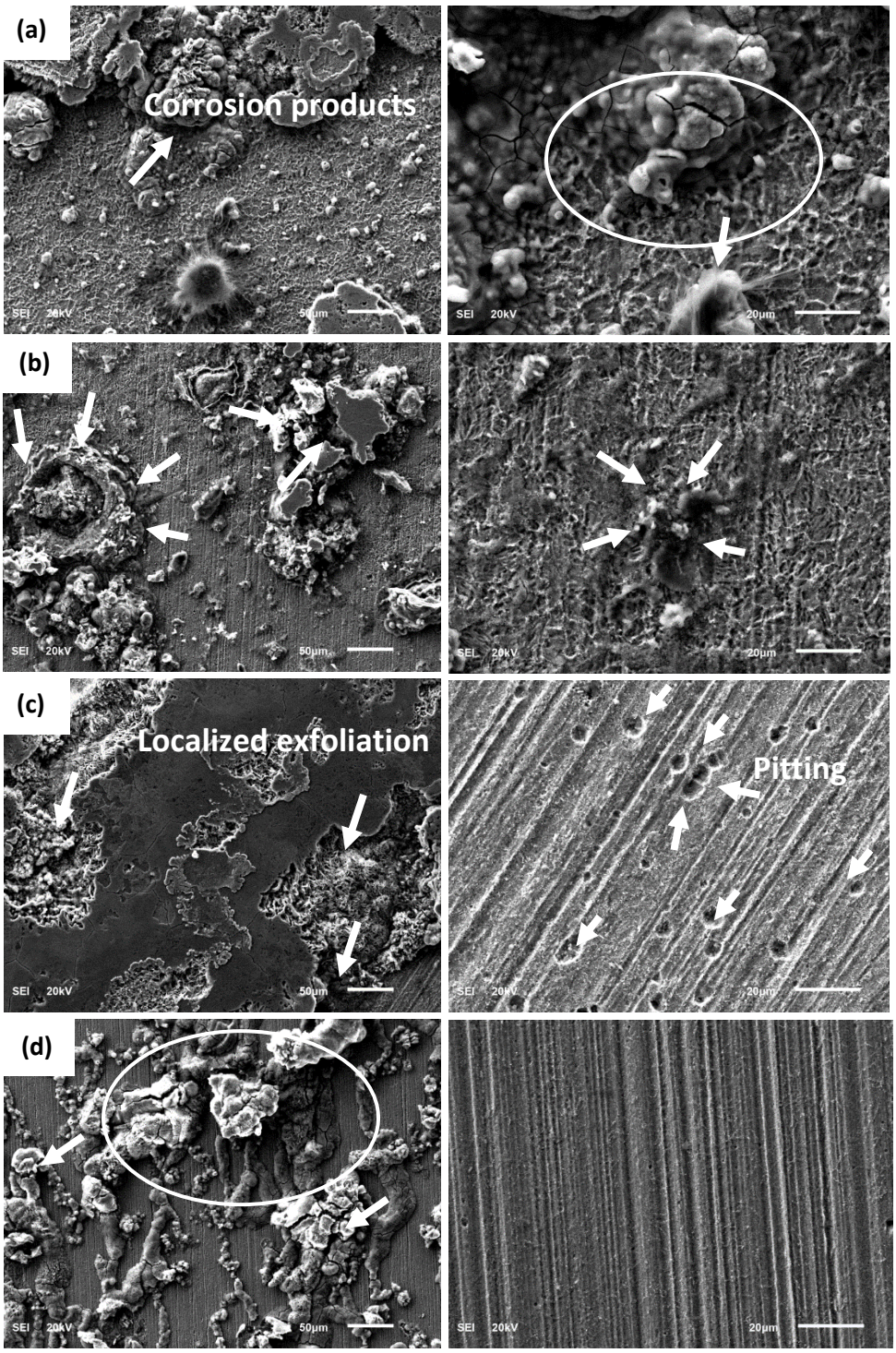

Figure 31: SEM micrographs of corrosion products formed on X60 pipeline steel exposed to (a) blank (corrodent) CO_2 saturated 3.5% NaCl solution; and the corrodent containing (b) 100 ppm Chitosan; (c) CMC; (d) commercial inhibitor at room temperature after 24 hr immersion. [Right and left panels show 50 and 20 µm micrographs, respectively].

4.6 Adsorption Isotherm

The experimental results obtained from the present study revealed the dependence of inhibition efficiency on the concentration of the inhibitor systems, and since corrosion inhibition is attributable to the molecular adsorption of inhibitor components at the metal surface—either directly or by the formation of films—various adsorption isotherm models (AIMs) could be deployed to explain this phenomenon. These models provide information on the interaction between adsorbed species at the metal/electrolyte interface. The magnitude of surface coverage (θ) from the EIS measurements obtained using equation 4.13 (assuming a direct relation between surface coverage (θ) and inhibition efficiency (IE%) was employed for a particular range of inhibitor concentrations [71]:

$$IE\% = \theta \times 100 \tag{4.12}$$

By fitting the experimentally derived surface coverage values (obtained from Equation 4.12) with various AIMs, the model will be adopted that best matches the data by virtue of evaluating the closeness of values of correlation coefficient (R^2) to unity. In this study, the experimental data best fit the Langmuir adsorption model (mathematically expressed in Equation 4.13). The Langmuir adsorption isotherm postulates the uniequivalence inhibitor adsorption sites of surfaces, as well as the independency in molecular adsorption with the number of available sites [72,73]:

$$\frac{C}{\theta} = C + \frac{1}{K_{ads}} \tag{4.13}$$

$K_{ads} = Equilibrium\ constant\ associated\ with\ the\ interfacial\ molecular\ adsorption$
$C = Inhibitor\ concentration\ (measured\ in\ ppm)$
$\theta = Magnitude\ of\ the\ surface\ coverage\ of\ individual\ inhibitors\ on\ the\ pipe\ steel$

The Langmuir plot, as C/θ vs. C, is shown to be linear in Figure 32, indicating that molecular adsorption of chitosan, CMC, and the commercial inhibitor on the surface of the X60 pipeline steel substrate within the range of concentrations of the inhibitors studied at 25°C could be approximated by this adsorption isotherm model. The adsorption parameters derived from the adsorption isotherm plot are listed in Table 12.

Although the magnitude of correlation coefficient (R^2) is approximately unity, which is indicative of a good fitting (Table 12), the gradients of the plot for each inhibitor are greater than unity, which opposes the monolayer molecular adsorption phenomenon previously proposed by the Langmuir adsorption isotherm model. This considerable deviation of the slope from unity may be attributed to the abundance of molecular interactions of several adsorbed species at the metal/solution interface, since perfect homogenous adsorption sites are not likely to exist in corrosion systems. This calls for a redefining of the Langmuir adsorption isotherm by introducing a dimensionless separation constant (K_L) (Equation 4.14) [74]:

$$\mathrm{K_L} = 1/(1 + \mathrm{K_{ads}C}) \tag{4.14}$$

For each concentration of corrosion inhibitor molecule, the calculated values of this dimensionless quantity are presented in Table 13. The presented values of K_L for the single-component inhibitors and the commercial inhibitor are all less than unity ($K_L < 1$), thus showing favorable molecular adsorption and good fitting for the range of concentrations of the inhibitors being studied [74].

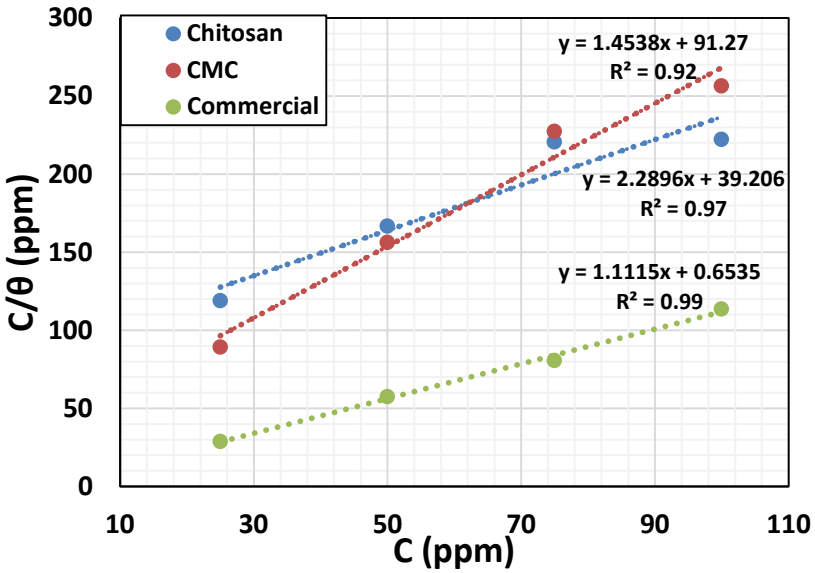

Figure 32: Langmuir adsorption isotherm for the test inhibitors on X60 pipeline steel immersed in CO_2-saturated 3.5% NaCl solution at 25°C obtained from the EIS measurements.

The magnitude of K_{ads} in Equations 4.12 and 4.13 is empirically related to the standard Gibbs energy (ΔG^{o}_{ads}) of adsorption by Equation 4.15 [75]:

$$\Delta G^{o}_{ads} = -RT\ In\ (1 \times 10^{6}\ K_{ads}) \qquad (4.15);$$

where the absolute temperature, T, is measured in K; the molar gas constant, R, is expressed in J/K/mol; and the magnitude of the concentration of water molecules, 1×10^{6}, is expressed in mg/L (ppm). The adsorption parameters derived from the Langmuir adsorption isotherm (Figure 32) are listed in Table 12, with values of K_{ads} recorded as 0.03, 0.01, and 1.53, respectively, for chitosan, CMC, and the commercial inhibitor; this is indicative of a stronger binding form of the components of the commercial inhibitor compared to the single component molecules.

Table 12: Langmuir adsorption parameters for X60 pipeline steel corrosion in the presence of the inhibitor systems in CO2-saturated 3.5% NaCl solution.

Inhibitor	ΔG^{o}_{ads} (kJ/mol)	K_{ads} ($g^{-1}L$)	Slope	R^2
Chitosan	– 25.14	0.03	2.29	0.97
CMC	– 23.03	0.01	1.45	0.92
Commercial	– 35.28	1.53	1.11	0.99

Table 13: Values of dimensionless separation constant (K_L), derived from the Langmuir adsorption isotherm for chitosan, CMC, and the commercial inhibitor.

Inhibitor Concentration (ppm)	Chitosan K_L	CMC K_L	Commercial K_L
25	0.7850	0.6106	0.0254
50	0.6461	0.4395	0.0129
75	0.5489	0.3433	0.0086
100	0.4772	0.2817	0.0065

The range of values of ΔG_{ads} (–25.14, –23.03, and –35.28 kJ/mol, respectively, for chitosan, CMC, and the commercial inhibitor) is suggestive of physisorption (electrostatic metal-inhibitor interaction for chitosan and CMC) and a mixed physisorption–chemisorption for the commercial inhibitor. Normally, ΔG_{ads} values up to –20 kJ/mol are consistent with a physical adsorption mechanism, while those lower than –40 kJ/mol define a chemical adsorption mechanism [76]. The negative magnitude of ΔG_{ads} is indicative of thermodynamic spontaneity associated with the adsorption process of the inhibitors onto the X60 pipeline steel surface. The physical adsorption mechanism proposed for chitosan and CMC indicates an electrostatic interaction between charged molecules at the metal surface and molecular desorption from the metal surface as the temperature is raised; this is consistent with the experimental electrochemical data.

CHAPTER 5

CONCLUSIONS

The performance of two green inhibitors—chitosan and carboxymethyl cellulose (CMC)— and one commercial inhibitor, on a typical X60 pipeline steel in CO_2-saturated 3.5% NaCl solution were investigated in both static and dynamic conditions, using electrochemical impedance spectroscopy (EIS) and potentiodynamic polarization (PDP) techniques. From the results obtained, the following conclusions can be drawn:

- The two green inhibitors were found to inhibit the corrosion of low-carbon X60 steel in CO_2-saturated 3.5% NaCl solution.
- Corrosion inhibition effect of all the investigated inhibitors was found to be concentration dependent. Inhibition efficiency increased with the increase of chitosan and CMC concentrations. For the commercial inhibitor, the optimum inhibition efficiency was obtained at 75 ppm concentration.
- Immersion time was found to have a profound effect on the corrosion inhibition performance of each inhibitor. Inhibition efficiency increased with prolonged immersion time for chitosan and commercial inhibitor while that of CMC decreased.

- Inhibition efficiency decreased with the increase in temperature from 25 to 40^{o}C and thereafter increased as the temperature was raised to 60^{o}C for all the inhibitors studied with pronounced effect noticed for the commercial inhibitor compared to chitosan and CMC.
- Potentiodynamic polarization measurements show that all inhibitors essentially acted as mixed-type inhibitors.
- Corrosion inhibition effect of chitosan, CMC and the commercial inhibitor for X60 steel in CO_2- saturated saline environment was afforded by virtue of the adsorption of each inhibitor on the steel surface which was found to follow Langmuir's adsorption isotherm model.
- With the protection of steel corrosion in CO_2-saturated saline solution to some extent at a concentration as low as 100 ppm for chitosan and CMC as standalone inhibitors, these organic compounds could, under appropriate formulation, serve as anticorrosive additives for low carbon steel corrosion in CO_2-saturated NaCl environments that could be as effective as the commercial inhibitor for practical industrial applications.

REFERENCES

[1] Killaars, J. and Finley, P. (2001) *SPE International Symposium on Oilfield Chemistry*. Houston, Texas, SPE 65044.

[2] Lopez, D. A., Schreiner, W. H., de Sanchez, S. R., and Simison, S. N. (2004) The influence of inhibitors molecular structure and steel microstructure on corrosion layers in CO_2 corrosion. *Applied Surface Science*, 236: 77-97.

[3] Fosbol, P. L. (2008) *Carbon dioxide corrosion: Modelling and experimental work applied to natural gas pipelines*. Ph.D. Thesis, Technical University of Denmark.

[4] Chong, L. (2009) *Effect of corrosion inhibitor on water wetting and carbon dioxide corrosion in oil-water two-phase flow*. Ph.D. Thesis, Ohio University.

[5] Fleming, N., Bourne, H. M, Strachan, C. J., and Buckley, A. S. (2001) *SPE International Symposium on Oilfield Chemistry*. Houston, Texas, SPE 65041.

[6] Dalmazzone, C. and Noik, C. (2001) *SPE International Symposium on Oilfield Chemistry*. Houston, Texas, SPE 65041.

[7] Obeyesekere, N., Naraghi, D., Abayarathna, R., Prasad, R., and Montgomerie, H. (2000) *NACE Corrosion 2000*, Paper No. 20, Houston, Texas.

[8] Koteeswaran, M. (2010) *CO_2 and H_2S corrosion in oil pipelines*. MS Thesis, University of Stavanger.

[9] Hunnik E. W., Pots, B. F., and Hendriksen, E. L. (1996) The formation of protective FeCO3 corrosion product layers in CO_2 corrosion. *Corrosion/96*, Paper No.6.

[10] Gray, et al. (1990) Effect of pH and temperature on the mechanism of carbon steel corrosion by aqueous carbon dioxide. *Corrosion/90*, Paper No.40.

[11] Baylis, J. R. (1926) Factors other than dissolved oxygen influencing the corrosion of iron pipes. *Journal of Industrial and Engineering Chemistry*, 18(4), 370-380.

[12] Xia, Z., Chou, K. C., and Szklarska-Smialowska, Z. (1989) Pitting corrosion of carbon steel in carbon dioxide-containing sodium chloride brine. *Corrosion 45*(8), 636-642.

[13] Yuhua, S. and Nesic, S. (2004) A parametric study and modeling on localized CO_2 corrosion in horizontal wet gas flow. *Corrosion/04*, Paper No. 380.

[14] Kvarekval, J. (2007) Morphology of localised corrosion attacks in sour environments. *Corrosion/07*, Paper No. 659.

[15] Feigel, R. E., Hayden, L. E., and Gomez, G. J. (1991) *Manual for determining the remaining strength of corroded pipe—A supplement for the ASME B31 pressure piping*. ASME B31G.

[16] Damage mechanisms affecting fixed equipment in the refining industry. (2011) *API Recommended Practice 571*, 2nd Edition.

[17] Hayduk, W. and Malik, V. K. (1971) Density, viscosity, and carbon dioxide solubility and diffusivity in aqueous ethylene glycol solutions. *Journal of Chemical & Engineering Data*, 16(2), 143-146.

[18] Huot, J. Y., Battistel, E., Lumry, R., Villeneuve, G., Lavallee, J. F., Anusiem, A., and Jolicoeur, C. (1988) A comprehensive thermodynamic investigation of water-ethylene glycol mixtures at 5, 25, and 45°C. *Journal of Solution Chemistry*, *17*(7), 601-636.

[19] Kapadi, U. R., Hundiwale, D. G., Patil, N. B., Patil, P. R., and Lande, M. K. (2000) Densities, excess molar volumes, viscosities of binary mixtures of ethanediol with water. *Journal of the Indian Chemical Society*, 77; 319-321.

[20] Saji, V. S. (2010) A review on recent patents in corrosion inhibitors. *Recent Patents on Corrosion Science*, 2, 6-12.

[21] Protopopoff E, Marcus P (1995) Electrochemistry and materials science of cathodic hydrogen absorption and adsorption, PV 94-21. Conway, BE, Jerkiewicz, G, *Journal of the Electrochemical Society*, NJ 374-386.

[22] Kesavan, D., Gopiraman, M, and Sulchana, N. (2012) Green inhibitors for corrosion of metals: A review. *Chemical Science Review and Letters*, *1*(1), 1-8.

[23] Umoren S. A., Ogbobe O., Igwe I. O., and Ebenso E. E. (2008) Inhibition of mild steel corrosion in acidic medium using synthetic and naturally occurring polymers and synergistic halide additives. *Corrosion Science, 50: 1998–2006*.

[24] Umoren, S. A., Obotl, I. B., Ebenso, E. E., and Okafor, P. C. (2008) Eco-friendly inhibitors from naturally occurring exudate gums for aluminium corrosion inhibition in acidic medium. *Portugaliae Electrochimica Acta*, 26: 267-282.

[25] Bayol, E., Gürten, A. A., Dursun, M., and Kayakirilmaz, K. (2008) Adsorption behavior and inhibition corrosion effect of sodium carboxymethyl cellulose on mild steel in acidic medium. *Acta Physico-Chimica Sinica*, 24: 2236-2243.

[26] Solomon, M. M., Umoren, S. A., Udosoro, I. I., and Udoh, A. P. (2010) Inhibitive and adsorption behaviour of carboxymethyl cellulose on mild steel corrosion in sulphuric acid solution. *Corrosion Science*, 52: 1317-1325.

[27] Umoren, S. A., Solomon, M. M., Udosoro, I. I., and Udoh, A. P. (2010) Synergistic and antagonistic effects between halide ions and carboxymethyl cellulose for the corrosion inhibition of mild steel in sulphuric acid solution. *Cellulose*, 17: 635-648.

[28] Arukalam, I. O. (2012) The inhibitive effect of hydroxyethylcellulose on mild steel corrosion in hydrochloric acid solution. *Academic Research International*, 2(*1*), 35-42.

[29] Chen, H. J. (1999) Effects of multiphase flow on corrosion inhibitor. *Corrosion 99*, Paper No. 10, Houston, Texas.

[30] Chen, H. J. (2002) Environmentally friendly inhibitors for CO_2 corrosion. *Corrosion Journal*, Paper No. 2300.

[31] Martinez, S., and Stern, I. (2001) Inhibitory mechanism of low-carbon steel corrosion by mimosa tannin in sulphuric acid solutions. *Journal of Applied Electrochemistry*, 31: 973-978.

[32] Abdallah, M. (2004) Guar gum as corrosion inhibitor for carbon steel in sulfuric acid solutions. *Portugaliae Electrochimica Acta*, 22: 161-175.

[33] Mobin, M., Khan, M. A., and Parveen, M. (2011) Inhibition of mild steel corrosion in acidic medium using starch and surfactants additives. *Journal of Applied Polymer Science*, 121: 1558-1565.

[34] Anthonsen, M. W., Varum, K. M., and Smidsrod, O. (1993) Solution properties of chitosans: Conformation and chain stiffness of chitosans with different degrees of *N*-acetylation. *Carbohydrate Polymers*, 22: 193-201.

[35] Wang, W., Bo, S., Li, S., and Qin, W. (1991) Determination of the Mark-Houwink equation for chitosan with different degrees of deacetylation. *International Journal of Biological Macromolecules*, 13: 281-285.

[36] El-Haddad, M. (2013) Chitosan as a green inhibitor for copper corrosion in acidic medium. *International Journal of Biological Macromolecules*, 55: 142-149.

[37] Wang, B., Du, M., Zhang, J., and Gao, C. J. (2011) Electrochemical and surface analysis studies on corrosion inhibition of Q235 steel by imidazoline derivative against CO_2 corrosion. *Corrosion Science*, 53: 353-361.

[38] Heydari, M. and Javidi, M. (2012) Corrosion inhibition and adsorption behaviour of an amido-imidazoline derivative on API 5L X52 steel in CO2-saturated solution and synergistic effect of iodide ions. *Corrosion Science*, 61: 148-155.

[39] Okafor, P. C., Liu, X., and Zheng, Y. G. (2009) Corrosion inhibition of mild steel by ethylamino imidazoline derivative in CO_2-saturated solution. *Corrosion Science*, 51: 761-768.

[40] Desimone, M. P., Gordillo, G., and Simison, S. N. (2011) The effect of temperature and concentration on the corrosion inhibition mechanism of an amphiphilic amido-amine in CO_2-saturated solution. *Corrosion Science*, 53: 4033-4043.

[41] Ghareba, S. and Omanovic, S. (2011) The effect of electrolyte flow on the performance of 12-aminododecanoic acid as a carbon steel corrosion inhibitor in CO_2-saturated hydrochloric acid. *Corrosion Science*, 53: 3805-3812.

[42] Nam N. D., Somers, A., Mathesh, M., Seter, M., Hinton, B., Forsyth, M., and Tan, M. Y. J. (2014) The behaviour of praseodymium 4-hydroxycinnamate as an inhibitor for carbon dioxide corrosion and oxygen corrosion of steel in NaCl solutions. *Corrosion Science*, 80: 128-138.

[43] Jiang, X., Zheng, Y. G., and Ke, W. (2005) Effect of flow velocity and entrained sand on inhibition performances of two inhibitors for CO_2 corrosion of N80 steel in 3% NaCl solution. *Corrosion Science*, 47: 2636-2658.

[44] Jevremovic, I., Singer, M., dan-Nešic, S., and Stankovic, V. M. (2013) Inhibition properties of self-assembled corrosion inhibitor talloil diethylenetriamine

imidazoline for mild steel corrosion in chloride solution saturated with carbon dioxide. *Corrosion Science*, 77: 265-272.

[45] Nam, N. D., Bui, Q. V., Mathesh, M., Tan, M. Y. J., and Forsyth, M. (2013) A study of 4-carboxyphenylboronic acid as a corrosion inhibitor for steel in carbon dioxide containing environments. *Corrosion Science*, 76: 257-266.

[46] Jawich, M. W. S., Oweimreen, G. A., and Ali, S. A. (2012) Heptadecyl-tailed mono- and bis-imidazolines: A study of the newly synthesized compounds on the inhibition of mild steel corrosion in a carbon dioxide–saturated saline medium. *Corrosion Science*, 65: 104-112.

[47] Lopez, D. A., Simison, S. N., and de Sanchez, S. R. (2005) Inhibitors performance in CO_2 corrosion EIS studies on the interaction between their molecular structure and steel microstructure. *Corrosion Science*, 47: 735-755.

[48] Khodyrev, Y. P., Batyeva, E. S., Badeeva, E. K., Platova, E. V., Tiwari, L., and Sinyashin, O. G. (2011) The inhibition action of ammonium salts of O,O'-dialkyldithiophosphoric acid on carbon dioxide corrosion of mild steel. *Corrosion Science*, 53: 976-983.

[49] Azghandi, M. V., Davoodi, A., Farzi, G. A., and Kosari, A. (2012) Water-base acrylic terpolymer as a corrosion inhibitor for SAE1018 in simulated sour petroleum solution in stagnant and hydrodynamic conditions. *Corrosion Science*, 64: 44-54.

[50] Zhao, J. and Chen, G. (2012) The synergistic inhibition effect of oleic-based imidazoline and sodium benzoate on mild steel corrosion in a CO2-saturated brine solution. *Electrochimica Acta*, 69: 247- 255.

[51] Mazumder, M. A. J., Al-Muallem, H. A., Faiz, M., and Ali, S. A. (2014) Design and synthesis of a novel class of inhibitors for mild steel corrosion in acidic and carbon dioxide-saturated saline media. *Corrosion Science*, 87: 187-198.

[52] Mazumder, M. A. J., Al-Muallem, H. A., and Ali, S. A. (2015) The effects of N-pendants and electron-rich amidine motifs in 2-(p-alkoxyphenyl)-2-imidazolines on mild steel corrosion in CO_2-saturated 0.5 M NaCl. *Corrosion Science*, 90: 54-68.

[53] Farelas, F. and Ramirez, A. (2010) Carbon dioxide corrosion inhibition of carbon steels through bis-imidazoline and imidazoline compounds studied by EIS. *International Journal of Electrochemical Science*, 5: 797-814.

[54] Sahin, M. and Bilgic, S. (2003) The inhibition effects of some heterocyclic nitrogenous compounds on the corrosion of the steel in CO2-saturated NaCl solutions. *Anti-Corrosion Methods and Materials*, 50(*1*): 34-39.

[55] Okafor, P. C., Liu, C. B., Liu, X., Zheng, Y. G., Wang, F., Liu, C. Y., and Wan, F. (2010) Corrosion inhibition and adsorption behavior of imidazoline salt on N80 carbon steel in CO_2-saturated solutions and its synergism with thiourea. *Journal of Solid State Electrochemistry*, 14: 1367-1376.

[56] Ahmed, A., Rasha, R., Farghali, R. A., and Fekry, A. M. (2012) Study for the stability and corrosion inhibition of electrophoretic deposited chitosan on mild steel alloy in acidic medium. *International Journal of Electrochemical Science*, 7: 7270-7282.

[57] Fekery, A. M. and Mohamed, R. R. (2010) Acetyl thiourea chitosan as an eco-friendly inhibitor for mild steel in sulphuric acid medium. *Electrochim Acta*, 55: 1933-1939.

[58] Li, M., Xu, J., Li, R., Wang, D., Li, T., Yuan, M., and Wang, J. (2014) Simple preparation of aminothiourea-modified chitosan as corrosion inhibitor and heavy metal ion adsorbent. *Journal of Solid State Electrochemistry*, 417: 131-6.

[59] Umoren, S. A., Gasem, Z. M., and Obot, I. B. (2013) Natural products for material protection: Inhibition of mild steel corrosion by date palm seed extracts in acidic media. *Industrial & Engineering Chemistry Res*earch, 52, 14855-14865.

[60] Okafor, P. C. and Zheng, Y. (2009) Synergistic inhibition behaviour of methylbenzyl quaternary imidazoline derivative and iodide ions on mild steel in H2SO4 solutions. *Corrosion Sci*ence, 51, 850-859.

[61] Abd El Rehim, S. S., Hassan, H. H., and Amin, M. A. (2001) Corrosion inhibition of aluminum by 1,1(lauryl amido)propyl ammonium chloride in HCl solution. *Materials Chemistry and Physics* 70: 64-72.

[62] Umoren, S. A., Li, Y., and Wang, F. H. (2010) Synergistic effect of iodide ion and polyacrylic acid on corrosion inhibition of iron in H_2SO_4 investigated by electrochemical techniques. *Corrosion Science*, 52: 2422-2429.

[63] Yasakau, K. A., Carneiro, J., Zheludkevich, M. L., and Ferreira, M. G. S. (2014) Influence of sol-gel process parameters on the protection properties of sol-gel coatings applied on AA2024, *Surface & Coatings Technology*, 246: 6-16.

[64] Kirtay, S. (2014) Preparation of hybrid silica sol-gel coatings on mild steel surfaces and evaluation of their corrosion resistance. *Progress in Organic Coatings*, 77: 1861-1866.

[65] Ruhi, G., Modi, O. P., Sinha, A. S. K., and Singh, I. B. (2008) Effect of sintering temperatures on corrosion and wear properties of sol-gel alumina coatings on surface pre-treated mild steel. *Corrosion Science*, 50: 639-649.

[66] Jiang, X., Zheng, Y. G., and Ke, W. (2005) Effect of flow velocity and entrained sand on inhibition performances of two inhibitors for CO_2 corrosion of N80 steel in 3% NaCl solution. *Corrosion Science* 47: 2636-2658.

[67] De Waard, C., Milliams, D. E. (1975) Carbonic acid corrosion of steel. *Corrosion* 31: 177-181.

[68] Lopes-Sesenes, R., Dominguez-Patiño, G. F., Gonzalez-Rodriguez, J. G., and Uruchurtu-Chavarin, J. (2013) Effect of flowing conditions on the corrosion inhibition of carbon steel by extract of buddleia perfoliata. *International journal of Electrochemical Science*, 8: 477-489.

[69] Ko, M., Ingham, B., Laycock, N., and Williams, D. E. (2015) In situ synchrotron X-ray diffraction study of the effect of microstructure and boundary layer conditions on CO_2 corrosion of pipeline steels. *Corrosion Science*, 90: 192-201.

[70] Paolinelli, L. D., Brown, B., Simison, S. N., and Nesic, S. (2012) Inhibition of CO2 corrosion of carbon steel with 1% Cr. *Materials Chemistry and Physics*, 136: 1092-1102.

[71] Bouhrira, K., Chetouani, A., Zerouali, D., Hammouti, B., Yahyi, A., Et-Touhami, A., Yahyaoui, R., and Touzan, R. (2014) Theoretical investigation of inhibition of the corrosion of A106 steel in NaCl solution by di-n-butyl bis(thiophene-2-carboxylato-O,O0)tin(IV). *Research on Chemical Intermediates* 40: 569-586.

[72] Oguzie, E. E., Enenebeaku, C. K., Akalezi, C. O., Okoro, S. C., Ayuk, A. A., and Ejike, E. N. (2010) Adsorption and corrosion-inhibiting effect of Dacryodis edulis extract on low-carbon-steel corrosion in acidic media; *Journal of Colloid and Interface Sci*ence, 349: 283-292.

[73] Khaled, K. F. and El-Maghraby, A. (2014) Experimental, Monte Carlo and molecular dynamics simulations to investigate corrosion inhibition of mild steel in hydrochloric acid solutions. *Arabian Journal of Chemistry*, 7: 319-326.

[74] Noor, E. A. (2009) Evaluation of inhibitive action of some quaternary N-heterocyclic compounds on the corrosion of Al-Cu alloy in hydrochloric acid. *Materials Chemistry and Physics*, 114: 533-541.

[75] Umoren, S. A., Obot, I. B., Madhankumar, A., and Gasem, Z. M. (2015) Performance evaluation of pectin as ecofriendly corrosion inhibitor for X60 pipeline steel in acid medium: Experimental and theoretical approaches, Carbohydrate Polymers 124: 280-291.

[76] Bilgic, S., Sahin, M. (2001) The corrosion inhibition of austenitic chromium-nickel steel in H2SO4 by 2-butyn-1-ol. Materials Chemistry and Physics 70: 290-295.

[77] Waters, N., Connolly, R., Brown, D., Laskowski, B (2014) Electrochemical impedance spectroscopy for coating evaluation using a micro sensor. Annual Conference of the Prognostics And Health Management Society.

Vitae

Name	:Abdullah Ahmed Awdhah Al Shafloot AlAhmary
Nationality	:Saudi Arabia
Date of Birth	:8/2/1985
Email	:ahmaryaa@gmail.com
Address	:P. O. Box 18741 Dhahran 31311
Academic Background	:BSc in Mechanical Engineering, Newcastle University, UK